Immune Landscape of Invasive Ductal Carcinoma Tumour Microenvironment Identifies a Prognostic and Immunotherapeutically Relevant Gene Signature

Xuanwen Bao [1, 2*‡], Run Shi [3*], Kai Zhang [4], Shan Xin [1], Xin Li [5], Yanbo Zhao [4], Yanfang Wang [3‡]

1) Institute of Radiation Biology, Helmholtz Center Munich, German Research Center for Environmental Health, 85764 Neuherberg, Germany
2) Technical University Munich (TUM), 80333 Munich, Germany
3) Ludwig-Maximilians-Universität München (LMU), 80539 Munich, Germany
4) Department of Cardiology, Sir Run Run Shaw Hospital, Zhejiang University School of Medicine, 310016 Hangzhou, China
5) College of Life Sciences, Nanjing University, 210093, Nanjing, China

‡ Corresponding author:

Xuanwen Bao: xuanwen.bao@helmholtz-muenchen.de;

Yanfang Wang: yangfang.wang@cup.uni-muenchen.de

Email address: Xuanwen Bao: xuanwen.bao@helmholtz-muenchen.de; **Shan Xin:** shan.xin@helmholtz-muenchen.de; **Kai Zhang:** 3317020@zju.edu.cn; **Xin Li:** Shin_Lee@outlook.com; **Yanbo Zhao:** zhaoybzju@zju.edu.cn; **Run Shi:** Run.Shi@med.uni-muenchen.de; **Yanfang Wang:** yangfang.wang@cup.uni-muenchen.de.

Abstract

Background: Invasive ductal carcinoma (IDC) is a clinically and molecularly distinct disease. Tumour microenvironment (TME) immune phenotypes play crucial roles in predicting clinical outcomes and therapeutic efficacy.

Method: In this study, we depict the immune landscape of IDC by using transcriptome profiling and clinical characteristics retrieved from The Cancer Genome Atlas (TCGA) data portal. Immune cell infiltration was evaluated via single-sample gene set enrichment (ssGSEA) analysis and systematically correlated with genomic characteristics and clinicopathological features of IDC patients. Furthermore, an immune signature was constructed using the least absolute shrinkage and selection operator (LASSO) Cox regression algorithm. A random forest algorithm was applied to identify the most important somatic gene mutations associated with the constructed immune signature. A nomogram that integrated clinicopathological features with the immune signature to predict survival probability was constructed by multivariate Cox regression.

Results: The IDC were clustered into low immune infiltration, intermediate immune infiltration, and high immune infiltration by the immune landscape. The high infiltration group had a favourable survival probability compared with that of the low infiltration group. The low-risk score subtype identified by the immune signature was characterized by T cell-mediated immune activation. Additionally, activation of the interferon-α response, interferon-γ response and TNF-α signalling via the NFκB pathway was observed in the low-risk score subtype, which indicated T cell activation

and may be responsible for significantly favourable outcomes in IDC patients. A random forest algorithm identified the most important somatic gene mutations associated with the constructed immune signature. Furthermore, a nomogram that integrated clinicopathological features with the immune signature to predict survival probability was constructed, revealing that the immune signature was an independent prognostic biomarker. Finally, the relationship of VEGFA, PD1, PDL-1 and CTLA-4 expression with the immune infiltration landscape and the immune signature was analysed to interpret the responses of IDC patients to immune checkpoint inhibitor therapy.

Conclusion: Taken together, we performed a comprehensive evaluation of the immune landscape of IDC and constructed an immune signature related to the immune landscape. This analysis of TME immune infiltration patterns has shed light on how IDC respond to immune checkpoint therapy and may guide the development of novel drug combination strategies.

Keywords: immune landscape; immune signature; survival; invasive ductal carcinoma; immune checkpoint inhibitor

Introduction

Invasive ductal carcinoma (IDC) is a clinically and molecularly distinct disease. IDCs are typically of high histologic grade and high mitotic index. HER2 overexpression or amplification is detected in 20% of these tumours (1). IDC tends to

metastasize to bone, liver, and lung, whereas invasive lobular carcinoma (ILC) has a higher tendency to metastasize in gastrointestinal and genital tracts, serosal cavities, and meninges (2). IDCs usually form glandular structures in contrast to the small clusters formed by ILCs. The loss of CDH1 leads to the discohesive morphology in ILCs, whereas IDCs maintain intact cell adhesion (3). Furthermore, the frequency of recurrently mutated genes and recurrent copy-number alterations often differs significantly between IDCs and ILCs (3). These features are generally associated with a poor prognosis. Taken together, these differences suggest that ILCs and IDCs are distinct cancer types and progress along different pathways.

Genetic and epigenetic changes contribute to the progression of tumour progression and recurrence in different cancer types. However, accumulated evidence indicates that the tumour microenvironment (TME) has clinicopathological significance in predicting survival outcomes and assessing therapeutic efficacy factors (4, 5). TME cells constitute a vital element of cellular and noncellular components in the tumoural niche, including extracellular matrix and cellular components, such as fibroblasts, adipose cells, immune-inflammatory cells, and neuroendocrine cells. Previous studies have revealed that immune cells in the TME modulate cancer progression and are attractive therapeutic targets (6, 7). To date, the comprehensive landscape of immune cells infiltrating the TME of IDCs has not yet been elucidated. We propose that IDCs have a distinct immune landscape and that the immune landscape might lead to different prognoses and treatment responses. In this study, by applying several computational algorithms, we estimated the abundance of immune

cells in the TME of IDCs and analysed the correlation of the immune landscape with genomic characteristics and pathological features of IDCs. Furthermore, we built an immune signature based on the TME immune phenotype, which is a robust prognostic biomarker and predictive factor for the response to immune-checkpoint inhibitors.

Method

Data download

TCGA RNA-seq datasets and clinical data for IDCs were downloaded by UCSC Xena browser (https://xenabrowser.net/). GSE20685 and GSE86948 were downloaded from the Gene Expression Omnibus (GEO) database.

Implementation of Single-Sample Gene Set Enrichment Analysis (ssGSEA)

We obtained the marker gene set for immune cell types from Bindea et al (8). We used the ssGSEA program to derive the enrichment scores of each immune-related term. In brief, the infiltration levels of immune cell types were quantified by ssGSEA in the R package gsva (9). The ssGSEA applies gene signatures expressed by immune cell populations to individual cancer samples. The computational approach used in our study included 24 immune cells types that are involved in innate immunity and adaptive immunity. Tumours with qualitatively different immune cell infiltration patterns were grouped using hierarchical agglomerative clustering (based on Euclidean distance and Ward's linkage).

The T cell infiltration score (TIS) was defined as the average of the standardized values for CD8+ T, central memory CD4+ T, effector memory CD4+ T, central

memory CD8+ T, effector memory CD8+ T, Th1, Th2, Th17, and Treg cells. The obtained cytotoxic activity scores (CYT) score was calculated by the geometrical mean of PRF1 and GZMA (10). The CD8+ T/Treg ratio was the digital ratio of the ssGSEA scores for these two cell types. The correlation between risk score and immune cell ssGSEA score was calculated by Pearson correlation.

LASSO regularization

LASSO (least absolute shrinkage and selection operator) is an important regularization in many regression analysis methods (e.g., COX regression and logistic regression) (10). The idea behind LASSO is that an L1-norm is used to penalize the weight of the model parameters. Assuming a model has a set of parameters, the LASSO regularization can be defined as:

$$\lambda \cdot \sum_{i=0}^{n} \|w_i\|_1$$

It can also be expressed as a constraint to the targeted objective function:

$$\sum \|\boldsymbol{Y} - \boldsymbol{Y}^*\|_2 , \qquad s.t. \ \|w_i\|_1 < t$$

An important property of the LASSO regularization term is that it can force the parameter values to be 0, thus generating a sparse parameter space, which is a desirable characteristic for feature selection. In our analysis, 19 genes which highly associated with OS were used as the input.

Differentially expressed gene (DEG) analysis

DEG analysis was performed by the Limma package (11). The samples were separated into a high-risk score group and a low-risk score group. An empirical

Bayesian approach was applied to estimate the gene expression changes using moderated t-tests. The Q value (adjusted p value) for multiple testing was calculated using the Benjamini-Hochberg correction. The DEGs were defined as genes with a Q value less than 0.05. The clusterProfiler R package was applied for the GO analysis (12). GSEA was applied with the GSEA software.

Co-expression gene network based on RNA-seq data

The Weighted correlation network analysis (WGCNA) was used to construct the gene co-expression network (13). The co-expression similarity $s_{i,j}$ was defined as the absolute value of the correlation coefficient between the profiles of nodes i and j:

$$s_{i,j} = |cor(x_i, x_j)|$$

where x_i and x_j are expression values of for genes i and j, and $s_{i,j}$ represent Pearson's correlation coefficients of genes i and j, respectively.

A weighed network adjacency was defined by raising the co-expression similarity to a power β:

$$a_{i,j} = s_{i,j}^{\beta}$$

with $\beta \geq 1$. We selected the power of β = 5 and scale-free R^2 = 0.95 as the soft-thresholding parameters to ensure a signed scale-free co-expression gene network. Briefly, network construction, module detection, feature selection, calculations of topological properties, data simulation, and visualization were performed. Modules were identified via hierarchical clustering of the weighting coefficient matrix. The module membership of node i in module q was defined as:

$$K_{cor,i}^{(q)} := cor(x_i, E^{(q)})$$

where x_i is the profile of node i, and $\mathrm{E}(q)$ is the module eigengene (the first principal component of a given module) of module q. The module membership measure $K_{cor,i}^{(q)}$, lies in $[-1, 1]$ and specifies how close node i is to module q, $q = 1, \ldots, Q$.

By evaluating the correlations between the immune infiltration status, immune signature of IDCs and the module membership of each module, a brown module was selected for further analysis.

Statistical analysis

A random forest algorithm was applied to find the most important somatic mutation associated with the immune signature. Survival outcome analysis modelled the results in reference to the patient OS and RFS. P-values and Hazard ratios were obtained from univariate Cox proportional-hazards regression models using the R package survival. Multivariate Cox regression was used to calculate the coefficients in the nomogram. The nomogram was plotted by the rms package. The time-dependent AUC value was calculated by the survivalROC package.

Results

Immune Phenotype Landscape in the TME of IDC

Immune cell populations modulate diverse immune responses and lead to antitumour effects by infiltrating the IDC TME. The immune cell infiltration status was assessed by applying the ssGSEA approach to the transcriptomes of IDCs.

Twenty-four immune-related terms were incorporated to deconvolve the abundance of diverse immune cell types in IDCs. The IDCs were clustered into 3 clusters (low infiltration: 208; intermediate infiltration: 430; and high infiltration: 130) in terms of immune infiltration by applying an unsupervised clustering algorithm (Fig. 1A). By applying hierarchical cluster analysis and K-means clustering analysis, we constructed a TME cell network, depicting a comprehensive landscape of tumour-immune cell interactions and their effects on the OS of patients with IDC (Figs. 1B, S1 and S2). The TME immune cells were clustered into 4 clusters, and the correlation among different immune cell types is shown in Fig. 1B. The association of OS and RFS with different clusters of IDCs was analysed by a pairwise log-rank test. The results indicated that the high infiltration group had a favourable survival probability compared with that of the low infiltration group (Fig. 1C and 1D).

Construction of the immune signature

A total of 413 genes were involved in the 24 immune-related terms. We applied the univariate COX regression based on the survival datasets of patients with IDC and the expression profiles of the 413 genes. The 19 most significant genes were selected with the criteria of a p value less than 0.0005 (Fig. 2A). The expression profiles of the 19 genes are shown in Fig. 2B. LASSO Cox regression was performed on the 19 genes to identify the most important features in terms of predicting the survival of IDC patients (Fig. 2C, 2D and 2E). By forcing the sum of the absolute value of the regression coefficients to be less than a fixed value, certain coefficients were reduced to exactly zero, and the most powerful prognostic features (QRSL1, TIMM8A,

IGHA1, BATF, KLRB1, SPIB, and FLT3LG) were identified with relative regression coefficients. Cross-validation was applied to prevent over-fitting. A 7-gene immune signature was constructed according to the individual coefficients of the genes. Then, we calculated the risk score for each IDC patient and ranked them (Fig. 2F). Fig. 2G shows the survival overview in the IDC patients. A heatmap showed that patients in the high-risk group tended to have increased QRSL1 and TIMM8A expression levels, as well as decreased expression levels of IGHA1, BATF, KLRB1, SPIB, and FLT3LG (Fig. 2G). The Kaplan-Meier curve and Cox regression suggested that patients with high risk scores had significantly worse OS and RFS than those with low risk scores (HR=2.94, $p<0.0001$ and HR=2.28, $p=0.001$, respectively) (Fig. 2H and 2I). The effect of the 7 genes on the OS and RFS of IDC patients is shown in Fig. S3 and Fig. S4, respectively. To confirm our findings in the IDC cohort, we validated the prognostic function of the immune signature in two independent GEO cohorts (GSE20685 and GSE86948). The risk score was calculated for each patient by using the same formula as in the IDC cohort. The GSE20685 and GSE86948 cohorts were used to predict the OS of BRCA patients based on our immune signature model. Consistent with our previous findings, the Kaplan-Meier curve suggested a significantly better overall survival in the low-risk group than in the high-risk group (Fig. S5A and S5B).

The low risk score was associated with active infiltration status and high cytotoxic potential

High infiltration status showed a lower risk score than the intermediate

infiltration status and low infiltration status showed (Fig. 3A). Similarly, patients with a low risk score had a higher proportion of high immune infiltration than patients with a high risk score (Fig. 3B). The presence of high immune infiltration in patients was linked to a low risk score and was associated with a favourable outcome (Fig. 3C). To compare cytotoxic function with the immune landscape and immune signature that we constructed, the associated signatures were identified for each patient. IDCs with high infiltration status and low risk score were associated with increased levels of immune activation. The TIS ($p < 0.0001$ and $p < 0.0001$, respectively) (Fig. 3D and 3H), interferon-γ signature ($p < 0.0001$ and $p < 0.0001$, respectively) (Fig. 3E and 3I), and CYT ($p < 0.0001$ and $p < 0.0001$, respectively) (Fig. 3F and 3J) were increased in the low-risk score group and high infiltration group. The ssGSEA score of DCs was higher in the low-risk score group than in the high-risk score group. The Kaplan-Meier curve showed that in the low-risk score group, the ssGSEA score of DC cells affected survival but did not affect the high-risk score group (Fig. S6A, S6B and S6C). These data indicate that compared with high-risk score tumours, low-risk score tumours have a distinct immune phenotype, characterized by increased immune infiltration and increased levels of immune activation.

The low-risk score was associated with increased T cell infiltration

The association of risk score and immune-related cells was analysed by Pearson correlation. Cytotoxic cells, CD8+ T cells, T cells and the 6 other most significant immune-related cell types are shown in Fig. 4. A high level of correlation was found between the risk score and the T cell-mediated immune response. The ssGSEA scores

of 24 immune-related terms in the low, intermediate, and high immune status and low- and high-risk score groups are shown in Fig. S7A and S7C. The p value and difference in the mean ssGSEA score from the high- and low-infiltration status and low- and high-risk score groups are shown in Fig. S7B and Fig. S7D. The proportions of low, intermediate, and high immune infiltration status in different pathological subtypes and different AJCC stages of IDC are shown in Fig. S7E and Fig. S7F. The triple-negative subtype of IDCs had a higher proportion of high infiltration status IDCs than other pathological subtypes, indicating an active immune response in triple-negative IDCs. The risk score distribution in different pathological subtypes and different AJCC stages of IDC are shown in Fig. S5G and Fig. S5H. The luminal A subtype had a lower risk score than the other pathological subtypes.

Functional annotation and WGNCA of the transcriptomes of IDC patients

To identify the underlying biological characteristics of the constructed immune signature, DEG analysis was performed based on the high-risk score group and low-risk score group. The heatmap depicts the significant DEGs between the two groups (Fig. 5A). The GO analysis indicated that T cell activation, positive regulation of leukocyte cell-cell adhesion, and regulation of lymphocyte activation were the most significantly enriched biological processes between the high-risk score group and the low-risk score group (Fig. 5B). The GSEA results showed that allograft rejection, IL-6/JAK/STAT3 signalling, the inflammatory response, interferon-α response, interferon-γ response and TNF-α signalling via the NFκB pathway were the predominant upregulated pathways in the low-risk score group. In contrast, the E2F

targets, G2M checkpoints, MTORC1 signalling and protein secretion pathways were significantly downregulated in the low-risk score group (Fig. 5C and 5D). To further identify the underlying biological characteristics in the immune signature, WGCNA was performed, and the correlation of risk score and immune infiltration status with module membership was analysed. The soft threshold selection is shown in Fig. S8. The module-trait heatmap illustrates that the brown module had a significant p value with both immune signature and immune infiltration status (Fig. 5E); the coefficients were -0.64 and 0.8, respectively. The association between module membership and gene significance for each gene in the brown module is shown in Fig. 5F. The genes from the brown module with a coefficient greater than 0.5 were selected as hub genes, and GO enrichment analysis revealed that T cell activation and lymphocyte activation were the most significantly enriched biological processes, which further confirmed the results from the DEG analysis.

Mutation load and immune signature

The spectrum of somatic mutations in patients with IDCs is known to be varied. We next investigated the distributions of somatic mutations and observed different patterns among IDCs in terms of total mutation burden (TMB). The risk score from the immune signature had a positive correlation with TMB in IDC patients (Fig. 6A). By applying a random forest algorithm, we identified 35 highly variable mutated genes that were associated with the immune signature (Fig. 6B). TP53 was the predominant gene of the 35 identified genes.

Construction of a nomogram to predict overall survival in IDC patients

We constructed a nomogram that integrated clinicopathological features with the immune signature to predict the survival probability of IDC patients (Fig. 7A). The AUC(t) functions of the multivariable models were developed to indicate how well these features serve as prognostic markers. Compared to other features, such as signature-based risk score, AJCC-TNM stage and total mutation burden, the nomogram consistently showed the highest predictive power for overall survival in the follow-up period (Fig. 7B).

The immune signature predicted the immunotherapeutic benefits in IDC patients

VEGF-A, the main mediator in tumour angiogenesis, hinders T cell infiltration in the tumour microenvironment. Hence, we explored the correlation between VEGF-A expression and the T cell immune response in IDC tumours. Interestingly, the increased VEGFA expression significantly correlated with both decreased levels of activated CD8+ T cells and Th1 cell infiltration in the high immune infiltration tumour microenvironment but not in the low immune infiltration tumour microenvironment (Fig. 8A and 8B). Furthermore, perforin, the molecular effector found in the granules of cytotoxic T lymphocytes and natural killer cells, also showed a negative correlation with VEGF-A expression (Fig. 8C). Finally, the positive correlation of VEGF-A and the risk score was identified. PD-1, PDL-1 and cytotoxic T lymphocyte antigen-4 (CTLA-4) are promising targets for the treatment of patients with breast and non-small cell lung cancer. PD-1, PDL-1, and CTLA-4 antibodies are undergoing studies for the treatment of breast cancer. We analysed the correlation of PD-1, PDL-1, and CTLA-4 expression in the high- and low-infiltration groups. The

expression of PD-1, PDL-1, and CTLA-4 was more significantly correlated with CD8+ T cells, Th1 cell ssGSEA score and perforin expression in the high-infiltration group than in the low-infiltration group. Furthermore, the mean expression of PD-1, PDL-1, and CTLA-4 was significantly increased in the high-infiltration group, indicating a potentially enhanced response to the corresponding anticancer antibody for IDCs with high immune infiltration status. In our constructed immune signature, the risk score showed a negative correlation with PD-1, PDL-1, and CTLA-4 expression, which implies a potentially enhanced effect of PD-1, PDL-1, and CTLA-4 antibodies in patients with low risk score. Lastly, we checked the correlation of the expression profiles of several immune checkpoint proteins, e.g., CD160, CD274, CD276, CTLA-4, LAG3, and PDCD1, risk score, and VEGF-A in the TCGA and GSE20685 cohorts (Fig. S8).

Discussion

In this study, we depicted the immune landscape of IDC using a large cohort. The immune landscape might explain the differences in prognoses of patients with IDC and responses to PD1, PDL-1 and CTLA-4 antibodies. Based on the immune landscape, we constructed an immune signature that calculated the risk score per patient. The correlation of signature and immune landscape revealed that the T cell-mediated immune response played a crucial role in the signature. Patients with low risk scores had increased T cell infiltration scores, interferon-γ signatures, and cytotoxic activity scores, indicating active T cell immune responses and favourable

survival probability. A random forest algorithm was applied to find the most important somatic mutation correlated with the immune signature. A nomogram was constructed based on the immune signature and other clinicopathological properties of IDCs. A time-dependent ROC analysis showed high accuracy of the immune signature and nomogram in terms of predicting the survival of IDC patients. Lastly, PD-1, PDL-1, and CTLA-4 expression was found to be highly associated with the risk score. The patients with low risk scores had increased expression levels of PD-1, PDL-1, and CTLA-4, indicating a potentially high response rate to PD-1, PDL-1, and CTLA-4 antibodies.

In our analysis, the IDCs were clustered into three main clusters (low immune infiltration, intermediate immune infiltration, and high immune infiltration). The patients in the high-infiltration cluster had the best survival probability compared with patients in the low- and intermediate-infiltration clusters. The T cell immune response is the central event in antitumour immunity (14). T cells are divided into CD4+ (helper T cells, Th) and CD8+ (cytotoxic T cells, Tc) T cells. Their secretomes include IFN-γ, TNF-α, and IL17, which have antitumour effects. Hence, the increased T cell infiltration score, interferon-γ signature, and cytotoxic activity score may lead to an anti-tumour effect in the high-infiltration group. This finding could explain the different OS and RFS in the high- and low-infiltration groups.

From the immune landscape in IDCs, we built an immune signature that included seven features (QRSL1, TIMM8A, IGHA1, BATF, KLRB1, SPIB, and FLT3LG). FLT3LG is a crucial cytokine that controls the development of DCs and is particularly

346 important for CD8-positive classical DCs and their CD103-positive tissue
347 counterparts. A clinical trial is currently underway to treat melanoma patients with a
348 combination of immunostimulatory FLT3LG and a peptide-based vaccine targeting
349 DCs (15). KLRB1, which encodes CD161, a surface marker on several T cell subsets
350 and NK cells, has been found to be most frequently associated with favourable
351 outcomes in many cancer types by enhancing innate immune characteristics (16).
352 SPIB is a member of the ETS family and profoundly affects B cell functions. B cells
353 that lack SPIB fail to proliferate in response to IgM cross-linking, exhibit limited
354 capacity to respond to T-dependent antigens, and produce low levels of IgG1, IgG2a,
355 and IgG2b (17). In addition, SPIB can activate enhancer elements in both Ig-λ and
356 Ig-κ genes, increasing the expression of these two genes. BATF is an inhibitor of
357 AP-1-driven transcription. Recent studies have revealed that BATF can regulate
358 positive transcriptional activity in dendritic cells, B cells and T cells (18). BATF
359 leucine zipper motifs interact with interferon-regulatory factor 4 (IRF4) and IRF8 at
360 AP-1–IRF consensus elements (AICEs), adding additional flexibility to the actions of
361 IRF4 and IRF8, which were previously considered to interact with SPIB and PU.1
362 (19). The interaction of IRF4 and BATF in T helper 17 cells increases the
363 production of IL-17, IL-21, IL-22 and IL-23 receptor. TIMM8A is involved in the
364 import and insertion of hydrophobic membrane proteins from the cytoplasm to the
365 mitochondrial inner membrane. The Bax/Bak complex mediates the release of
366 DDP/TIMM8a and activates Drp1-mediated fission to promote mitochondrial
367 fragmentation and subsequent elimination during programmed cell death (20).

From the expression profiles of the seven genes above, we calculated the risk score for each patient and predicted the survival of IDC patients.

The risk score from the immune signature was most significantly correlated with the ssGSEA score of cytotoxic cells, CD8 T cells and T cells, indicating the important roles of the T cell immune response in the immune signature. Interestingly, DCs in the low-risk group played a more important role than DCs in the high-risk group. The increased proportion of DCs significantly correlated with favourable survival in the low-risk group but did not correlate with favourable survival of patients in the high-risk group. Th innate inflammatory cytokines, such as IL-1, IL-12, and IL-23 expressed by DCs, promote IFN-γ-secreting CD4+ T cell and cytotoxic T lymphocyte responses (21). The high proportion of DCs and T cells cooperate to achieve the antitumour effect in IDC patients with low risk scores. Furthermore, the GSEA results revealed high levels of IFN-γ, TNF-α, and TNF-α secretion in the low-risk group, which contribute to the antitumour activity in IDC patients with low risk scores. WGCNA revealed opposing directions of the risk score (cor = -0.64) and immune infiltration (cor = 0.8) with the brown module, indicating the high level of correlation of risk score (calculated by immune signature) and immune infiltration. The hub gene in the brown module plays an essential role in regulating immune infiltration. The GO analysis revealed that T cell activation was the most significantly enriched biological process, indicating that the T cell-mediated immune response is the central event in both immune infiltration and the immune signature.

The spectrum of somatic mutations varied in IDC patients. The different mutation

burdens in IDCs led us to analyse whether the landscape of immune cells and the immune signature were associated with somatic mutations. The TMB showed a positive correlation with the risk score in IDC patients. Furthermore, a random forest algorithm was performed to identify the most important variables correlated with the immune signature. TP53, SCN10A, PIK3CA and 32 other genes were the most significant variables in the analysis. TP53 and PIK3CA mutations are the most common gene mutations in IDCs (44% and 33%, respectively). In the 35 gene variables, GATA3, a key regulator of ER activity, is a newly identified gene that is mutated in IDCs (5% in ILC versus 13% in IDC, q = 0.03) (3). Mutations in GATA3 are more frequent in luminal A IDC and are mutually exclusive with FOXA1 events. The differential expression level and enrichment for mutations of GATA3 in IDCs and of FOXA1 in ILC indicates a preferential requirement for the distinct regulation of ER activity in ILC and IDC (3). Previous studies revealed that the GATA3 mutation correlates with increased expression, which is associated with the immune response (22, 23). Our analysis further confirms the correlation of the GATA3 mutation with immune infiltration. In addition, we constructed a nomogram that integrated clinicopathological features with the immune signature to predict the survival probability of IDC patients. Compared with other clinicopathological features, the immune signature showed the best accuracy in predicting the survival of IDC patients at any time point and would therefore be helpful for the diagnosis and precise treatment of IDC patients.

There have been several studies for the treatment of breast cancer with

412 immunotherapeutic antibodies. PD-1 is expressed by exhausted T cells. PD-1 and
413 PD-L1 exhibit inhibitory receptor–ligand interactions, which are involved in the
414 negative regulation of T cell activation and peripheral tolerance during immune
415 responses by cancer cells. Despite demonstrated successes, only a proportion of
416 patients benefit from PD-1 and PDL-1 antibody treatment. Hence, it is important to
417 determine the mechanism that leads to the varied therapeutic effect of PD-1 and
418 PDL-1 antibody treatment and thus improve individual diagnosis and precision
419 medicine. PD-L1 expression, microsatellite instability and deficient mismatch repair
420 are important biomarkers that predict the response to anti-PD-1/PD-L1 therapies
421 (24-26). Among the three biomarkers, PD-L1 expression has been validated in nearly
422 all tumour types for all approved anti-PD-1/PD-L1 therapies. In our analysis, the
423 expression of PD1, PDL-1, and CTLA-4 was significantly increased in the
424 high-infiltration group. Furthermore, the expression of PD1, PDL-1, and CTLA-4 had
425 a significant correlation with CD8+ T cells, Th1 cell ssGSEA score and perforin
426 expression in the high-infiltration group, which provides a basis for PD-1/PD-L1 and
427 CTLA-4 treatment. Similarly, the immune signature we constructed also indicated that
428 high expression levels of PD1, PDL-1, and CTLA-4 correlated with low risk score.
429 Therefore, patients with a low risk score could derive more benefit from
430 immunotherapy than patients with a high risk score.

431 In the current study, we performed a comprehensive evaluation of the immune
432 landscape of IDC and constructed an immune signature related to the immune
433 landscape. This analysis of TME immune infiltration patterns has shed light on how

IDC respond to immune checkpoint therapy and may guide the development of novel drug combination strategies.

List of abbreviations

TME: tumour microenvironment; IDC: invasive ductal carcinoma; TCGA: The Cancer Genome Atlas; GEO: Gene Expression Omnibus; ssGSEA: single-sample gene set enrichment; LASSO: least absolute shrinkage and selection operator; ILC: invasive lobular carcinoma; DEG: differentially expressed gene; WGCNA: weighted correlation network analysis; TMB: total mutation burden; IRF4: interferon-regulatory factor 4; AICE: AP-1–IRF consensus element.

Declarations

Ethics approval and consent to participate

Not applicable

Consent for publication

Not applicable

Availability of data and materials

The datasets supporting the conclusions of this article are available in the Xena browser (https://xenabrowser.net/) repository.

Competing interests

The authors declare that they have no competing interests.

Funding

This work was partially supported by the Zhejiang Provincial Natural Science Foundation (NO. LY16H020005).

Author Contributions

XW. B. and R. S. conceived and designed the experiments. XW. B., S. X., and K. Z. analysed the data. XW. B., and YF. W. wrote the paper. YB. Z., K. Z., and R. S. reviewed the draft. All authors read and approved the final manuscript.

Acknowledgements

We would like to thank Dr Michael Rosemann for helpful discussions and suggestions.

Figure legends

Fig. 1 Immune landscape of IDCs and the TME characteristics.

A, Unsupervised clustering of IDC patients from the TCGA cohort using ssGSEA scores from immune cell types. Mutation status of TP53, MYC, GATA3, MAP2K4, and CDH1, status of the oestrogen receptor, status of the progesterone receptor, status of Her2, survival, and stage are shown as patient annotations in the lower panel. Hierarchical clustering was performed with Euclidean distance and Ward linkage. Three distinct immune infiltration clusters, here termed high infiltration, median infiltration, and low infiltration, were defined. B, Interaction of the TME immune cell

types. The size of each term represents the survival impact of each TME cell type, calculated by $\log_{10}$ (log-rank test P value). The connection of TME immune cells represents interactions between both. The thickness of the line indicates the strength of the correlation calculated by Spearman correlation analysis. Positive correlations are represented in red, and negative correlations are represented in blue. The immune cell cluster was clustered by the hclust method. Immune cell cluster-A, yellow; cell cluster-B, blue; cell cluster-C, red; and cell cluster-D, brown. C, Kaplan-Meier curves for OS of IDC patients showing that the high immune infiltration group had a favourable outcome compared with the other groups. D, Kaplan-Meier curves for RFS of IDC patients showing that the high immune infiltration group had a favourable outcome compared with other groups. IDC: invasive ductal carcinoma; TME: tumour microenvironment; TCGA: The Cancer Genome Atlas; OS: overall survival; and RFS: recurrence-free survival.

Fig. 2 Signature-based risk score is a promising marker of survival in IDC patients.

A, The HR and P value from the univariable Cox HR regression of selected genes in the immune terms (Criteria: P value < 0.001). B, The expression of the selected genes shown by heatmap. Mutation status of TP53, MYC, GATA3, MAP2K4, and CDH1, status of the oestrogen receptor, status of the progesterone receptor, status of Her2, survival, and stage are shown as patient annotations in the lower panel. Hierarchical clustering was performed with Euclidean distance and Ward linkage. C and D, LASSO Cox analysis identified 7 genes most correlated with overall survival, and

10-round cross validation was performed to prevent overfitting. E, Coefficient distribution of the gene signature. F, Risk score distribution. G, Survival overview. H, Heatmap showing the expression profiles of the signature in the low- and high-risk groups. I, Patients in the high-risk group exhibited worse OS than those in the low-risk group. J, Patients in the high-risk group exhibited worse RFS than those in the low-risk group. IDC: invasive ductal carcinoma; OS: overall survival; and RFS: recurrence-free survival.

Fig. 3 Heterogeneous immune cell infiltration in the low- and high-risk score groups.

A, The distribution of risk scores in low, mediate and high immune infiltration patterns. B, The distribution of immune infiltration patterns in the low- and high-risk score groups. C, Alluvial diagram of immune infiltration patterns in groups with different risk scores and survival outcomes. D, TIS in low, mediate and high immune infiltration patterns. E, Relative interferon-γ signature in low, mediate and high immune infiltration patterns. F, Comparison of relative CYT in low, mediate and high immune infiltration patterns. G, Relative TIS in the low- and high-risk score groups. E, Relative interferon-γ signature in the low- and high-risk score groups. F, Comparison of relative CYT in the low- and high-risk score groups. TIS: T cell infiltration score; CYT: cytotoxic activity scores.

Fig. 4 The nine most significant correlations of risk score with immune cell infiltration ssGSEA score.

Fig. 5 Functional annotation of the immune signature and WGCNA of the IDC

transcriptome.

A, Heatmap showing the transcriptome expression profiles of the low- and high-risk groups. B, GO analysis based on the significant genes in the comparison between low- and high-risk groups. C and D, GSEA revealed that most significant hallmarks correlated with the immune signature. E, Correlation between modules and traits. G, The correlation between module membership and gene significance in the brown module. H, GO analysis based on the hub genes in the brown module. GO: gene ontology; GSEA: gene set enrichment analysis.

Fig. 6 The association of the immune signature with cancer somatic mutations.

A, The correlation between the immune signature and IDC somatic mutations. B, Distribution of somatic mutations correlated with the immune signature. The upper bar plot indicates OS and RFS per patient, whereas the left bar plot shows the importance of the somatic mutations correlated with the immune signature. IDC: invasive ductal carcinoma; OS: overall survival; and RFS: recurrence-free survival.

Fig. 7 Construction of a nomogram for survival prediction.

A, Nomogram combining the immune signature with clinicopathological features. B, The AUC(t) of the multivariable models indicated that the nomogram had the highest predictive power for overall survival.

Fig. 8 Immune signature predicts immunotherapeutic benefits

A, B and C, The correlation of VEGFA expression with T cell infiltration, Th1 cells and PRF1 expression in high and low immune infiltration conditions. D, The correlation of VEGFA expression with the immune signature. E, F and G, The

correlation of PD-1 expression with T cell infiltration, Th1 cells and PRF1 expression in high and low immune infiltration conditions. H, The correlation of PD-1 expression with the immune signature. I, J and K, The correlation of PDL-1 expression with T cell infiltration, Th1 cells and PRF1 expression in high and low immune infiltration conditions. L, The correlation of PDL-1 expression with the immune signature. M, N and O, The correlation of CTLA-4 expression with T cell infiltration, Th1 cells and PRF1 expression in high and low immune infiltration conditions. P, The correlation of CTLA-4 expression with the immune signature.

Fig. S1 The correlation between different infiltrating immune cells.

Fig. S2 The correlation between the ssGSEA scores of infiltrating immune cells and the OS probability of IDC patients.

Fig. S3 The correlation between the expression level of seven genes in the immune signature and the OS probability of IDC patients.

Fig. S4 The correlation between the expression of seven genes in the immune signature and the RFS probability of IDC patients.

Fig. S5 Validation of the immune signature in two external cohorts, GSE20685 (A) and GSE86948 (B).

Fig. S6 The correlation between the ssGSEA scores of DCs and the OS probability of IDC patients in the high- and low-risk score groups.

A, The ssGSEA scores were higher in the high- and low-risk score groups. B, The correlation between the ssGSEA scores of DCs and the OS probability of IDC patients in the low-risk score group. C, The correlation between the ssGSEA scores of DCs

and the OS probability of IDC patients in the high-risk score group.

Fig. S7 The ssGSEA score distribution in the low, intermediate and high immune infiltration patterns and in the low- and high-risk score groups.

A, The ssGSEA score distribution in low, intermediate and high immune infiltration patterns. B, The difference and P value from the comparison between the ssGSEA score from low and high immune infiltration patterns. C, The ssGSEA score distribution in the low- and high-risk score groups. D, The difference and P value from the comparison between the ssGSEA score from the low- and high-risk score group. E, The distribution of immune infiltration patterns in different pathological subtypes. F, The distribution of risk scores in different pathological subtypes. G, The distribution of immune infiltration patterns at different pathological stages. H, The distribution of risk scores at different pathological stages.

Fig. S8 The selection of the soft threshold in the WGCNA

Fig. S9 The correlation of the expression profiles of several immune checkpoint proteins, risk score, and VEGF-A in the TCGA (A) cohort and GSE20685 cohort (B).

References

1. Eble JN, Tavassoli FA, Devilee P. Pathology and genetics of tumours of the breast and female genital organs: Iarc; 2003.

2. Arpino G, Bardou VJ, Clark GM, Elledge RM. Infiltrating lobular carcinoma of the breast: tumor

characteristics and clinical outcome. Breast cancer research. 2004;6(3):R149.

3. Ciriello G, Gatza ML, Beck AH, Wilkerson MD, Rhie SK, Pastore A, et al. Comprehensive molecular portraits of invasive lobular breast cancer. Cell. 2015;163(2):506-19.

4. Smid M, Rodríguez-González FG, Sieuwerts AM, Salgado R, Prager-Van der Smissen WJ, van Der Vlugt-Daane M, et al. Breast cancer genome and transcriptome integration implicates specific mutational signatures with immune cell infiltration. Nature communications. 2016;7:12910.

5. Pages F, Galon J, Dieu-Nosjean M, Tartour E, Sautes-Fridman C, Fridman W. Immune infiltration in human tumors: a prognostic factor that should not be ignored. Oncogene. 2010;29(8):1093.

6. Keir ME, Butte MJ, Freeman GJ, Sharpe AH. PD-1 and its ligands in tolerance and immunity. Annu Rev Immunol. 2008;26:677-704.

7. Le DT, Uram JN, Wang H, Bartlett BR, Kemberling H, Eyring AD, et al. PD-1 blockade in tumors with mismatch-repair deficiency. New England Journal of Medicine. 2015;372(26):2509-20.

8. Bindea G, Mlecnik B, Tosolini M, Kirilovsky A, Waldner M, Obenauf AC, et al. Spatiotemporal dynamics of intratumoral immune cells reveal the immune landscape in human cancer. Immunity. 2013;39(4):782-95.

9. Hänzelmann S, Castelo R, Guinney J. GSVA: gene set variation analysis for microarray and RNA-seq data. BMC bioinformatics. 2013;14(1):7.

10. Rooney MS, Shukla SA, Wu CJ, Getz G, Hacohen N. Molecular and genetic properties of tumors associated with local immune cytolytic activity. Cell. 2015;160(1-2):48-61.

11. Smyth GK. Limma: linear models for microarray data. Bioinformatics and computational biology solutions using R and Bioconductor: Springer; 2005. p. 397-420.

12. Yu G, Wang L-G, Han Y, He Q-Y. clusterProfiler: an R package for comparing biological themes

608 among gene clusters. Omics: a journal of integrative biology. 2012;16(5):284-7.

609 13. Langfelder P, Horvath S. WGCNA: an R package for weighted correlation network analysis. BMC

610 bioinformatics. 2008;9(1):559.

611 14. Baeuerle PA, Reinhardt C. Bispecific T-cell engaging antibodies for cancer therapy. Cancer

612 research. 2009;69(12):4941-4.

613 15. Vacchelli E, Aranda F, Bloy N, Buqué A, Cremer I, Eggermont A, et al. Trial

614 Watch—Immunostimulation with cytokines in cancer therapy. Oncoimmunology. 2016;5(2):e1115942.

615 16. Gentles AJ, Newman AM, Liu CL, Bratman SV, Feng W, Kim D, et al. The prognostic landscape of

616 genes and infiltrating immune cells across human cancers. Nature medicine. 2015;21(8):938.

617 17. Gallant S, Gilkeson G. ETS transcription factors and regulation of immunity. Archivum

618 immunologiae et therapiae experimentalis. 2006;54(3):149-63.

619 18. Murphy TL, Tussiwand R, Murphy KM. Specificity through cooperation: BATF–IRF interactions

620 control immune-regulatory networks. Nature reviews immunology. 2013;13(7):499.

621 19. Li P, Spolski R, Liao W, Wang L, Murphy TL, Murphy KM, et al. BATF–JUN is critical for

622 IRF4-mediated transcription in T cells. Nature. 2012;490(7421):543.

623 20. Arnoult D, Rismanchi N, Grodet A, Roberts RG, Seeburg DP, Estaquier J, et al. Bax/Bak-dependent

624 release of DDP/TIMM8a promotes Drp1-mediated mitochondrial fission and mitoptosis during

625 programmed cell death. Current Biology. 2005;15(23):2112-8.

626 21. Butt A, Mills K. Immunosuppressive networks and checkpoints controlling antitumor immunity

627 and their blockade in the development of cancer immunotherapeutics and vaccines. Oncogene.

628 2014;33(38):4623.

629 22. Usary J, Llaca V, Karaca G, Presswala S, Karaca M, He X, et al. Mutation of GATA3 in human breast

630 tumors. Oncogene. 2004;23(46):7669.

631 23. Mantel P-Y, Kuipers H, Boyman O, Rhyner C, Ouaked N, Rückert B, et al. GATA3-driven TH2

632 responses inhibit TGF-β1–induced FOXP3 expression and the formation of regulatory T cells. PLoS

633 biology. 2007;5(12):e329.

634 24. Lee V, Le DT. Efficacy of PD-1 blockade in tumors with MMR deficiency. Future Medicine; 2016.

635 25. Diaz LA, Marabelle A, Delord J-P, Shapira-Frommer R, Geva R, Peled N, et al. Pembrolizumab

636 therapy for microsatellite instability high (MSI-H) colorectal cancer (CRC) and non-CRC. American

637 Society of Clinical Oncology; 2017.

638 26. Topalian SL, Hodi FS, Brahmer JR, Gettinger SN, Smith DC, McDermott DF, et al. Safety, activity,

639 and immune correlates of anti–PD-1 antibody in cancer. New England Journal of Medicine.

640 2012;366(26):2443-54.

641

642

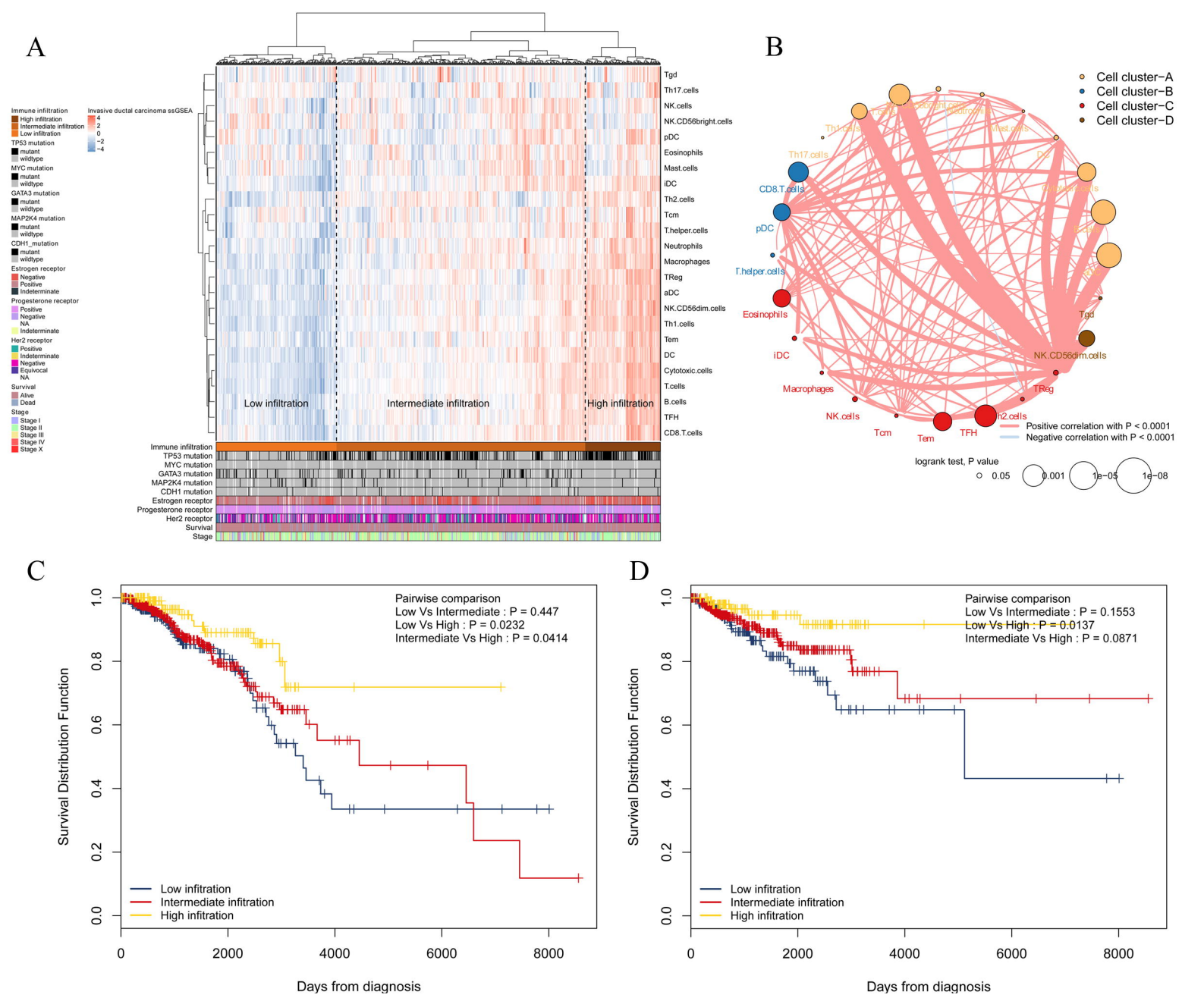
A
Immune infiltration
High infiltration
Intermediate infiltration
Low infiltration
TP53 mutation
mutant
wildtype
MYC mutation
mutant
wildtype
GATA3 mutation
mutant
wildtype
MAP2K4 mutation
mutant
wildtype
CDH1_mutation
mutant
wildtype
Estrogen receptor
Negative
Positive
Indeterminate
Progesterone receptor
Positive
Negative
NA
Indeterminate
Her2 receptor
Positive
Indeterminate
Negative
Equivocal
NA
Survival
Alive
Dead
Stage
Stage I
Stage II
Stage III
Stage IV
Stage X
Invasive ductal carcinoma ssGSEA
4
2
0
−2
−4
Tgd
Th17.cells
NK.cells
NK.CD56bright.cells
pDC
Eosinophils
Mast.cells
iDC
Th2.cells
Tcm
T.helper.cells
Neutrophils
Macrophages
TReg
aDC
NK.CD56dim.cells
Th1.cells
Tem
DC
Cytotoxic.cells
T.cells
B.cells
TFH
CD8.T.cells
Low infiltration
Intermediate infiltration
High infiltration
Immune infiltration
TP53 mutation
MYC mutation
GATA3 mutation
MAP2K4 mutation
CDH1 mutation
Estrogen receptor
Progesterone receptor
Her2 receptor
Survival
Stage
B
Cell cluster−A
Cell cluster−B
Cell cluster−C
Cell cluster−D
Th17.cells
CD8.T.cells
pDC
T.helper.cells
Eosinophils
iDC
Macrophages
NK.cells
Tcm
Tem
TFH
Tgd
NK.CD56dim.cells
TReg
Positive correlation with P < 0.0001
Negative correlation with P < 0.0001
logrank test, P value
0.05
0.001
1e−05
1e−08
C
Survival Distribution Function
Pairwise comparison
Low Vs Intermediate : P = 0.447
Low Vs High : P = 0.0232
Intermediate Vs High : P = 0.0414
Low infiltration
Intermediate infiltration
High infiltration
Days from diagnosis
D
Survival Distribution Function
Pairwise comparison
Low Vs Intermediate : P = 0.1553
Low Vs High : P = 0.0137
Intermediate Vs High : P = 0.0871
Low infiltration
Intermediate infiltration
High infiltration
Days from diagnosis

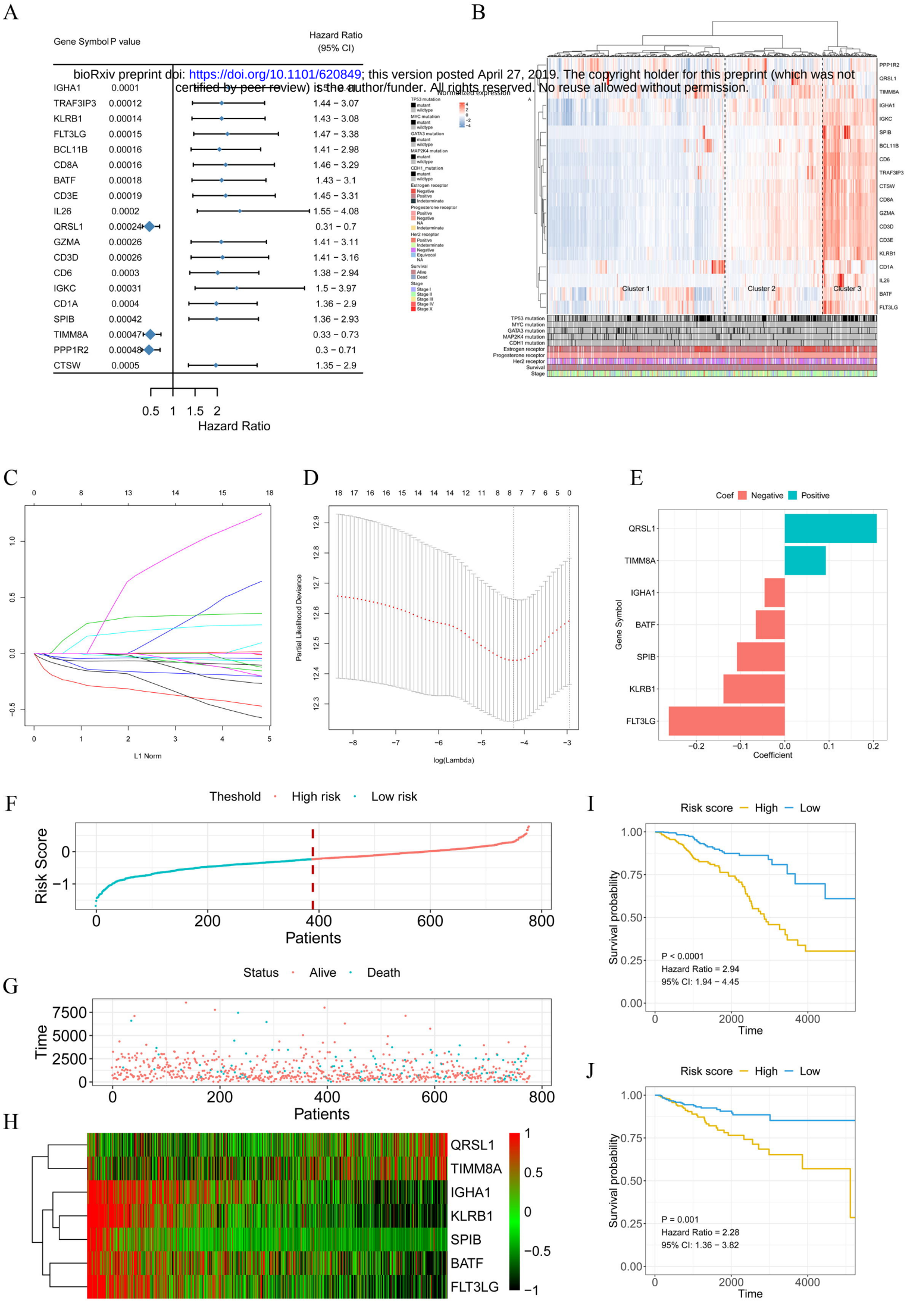

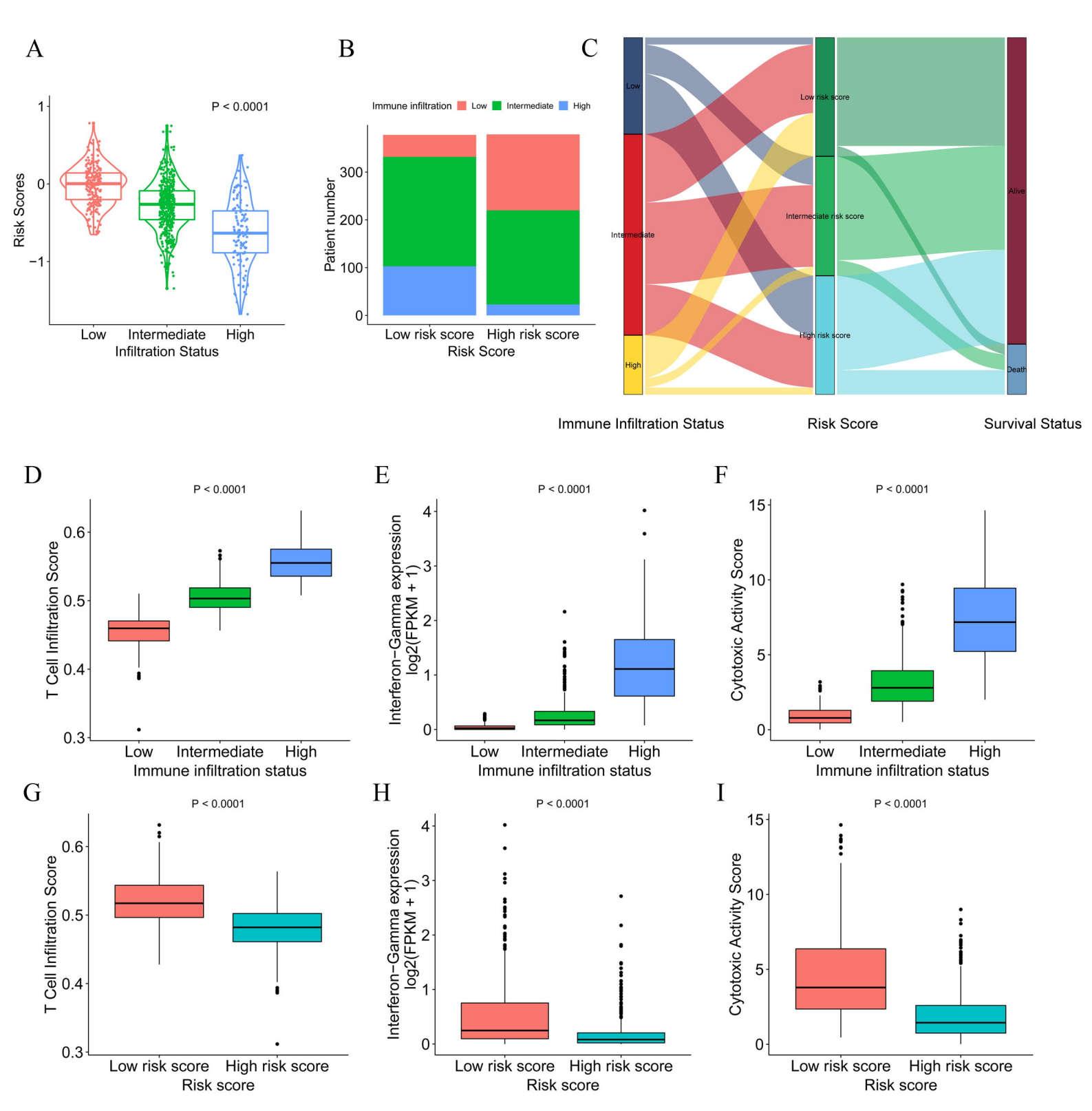
A
P < 0.0001
Risk Scores
Low
Intermediate
High
Infiltration Status
B
Immune infiltration Low Intermediate High
Patient number
Low risk score
High risk score
Risk Score
C
Low
Intermediate
High
Low risk score
Intermediate risk score
High risk score
Alive
Death
Immune Infiltration Status
Risk Score
Survival Status
D
P < 0.0001
T Cell Infiltration Score
Low
Intermediate
High
Immune infiltration status
E
P < 0.0001
Interferon−Gamma expression log2(FPKM + 1)
Low
Intermediate
High
Immune infiltration status
F
P < 0.0001
Cytotoxic Activity Score
Low
Intermediate
High
Immune infiltration status
G
P < 0.0001
T Cell Infiltration Score
Low risk score
High risk score
Risk score
H
P < 0.0001
Interferon−Gamma expression log2(FPKM + 1)
Low risk score
High risk score
Risk score
I
P < 0.0001
Cytotoxic Activity Score
Low risk score
High risk score
Risk score

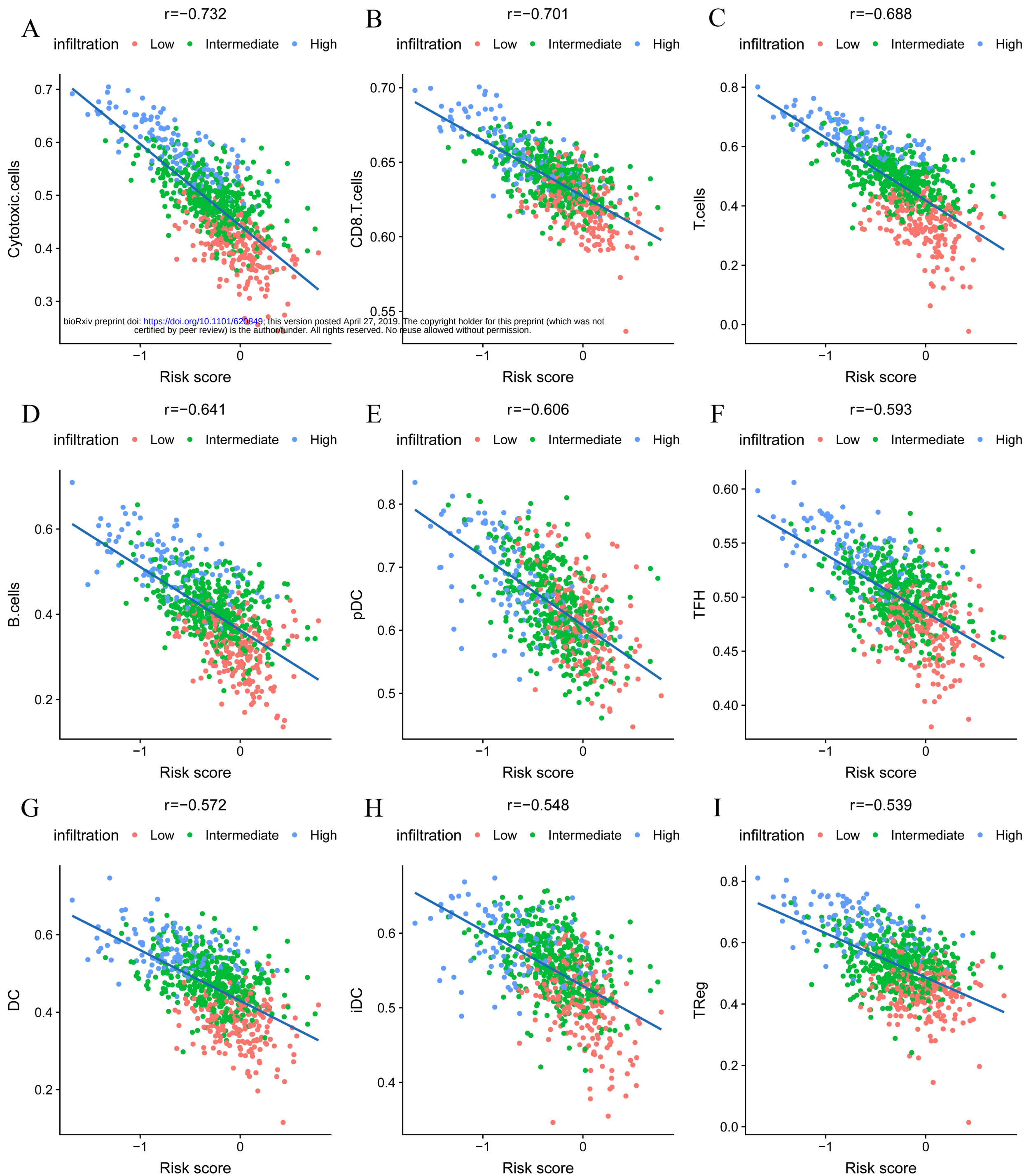

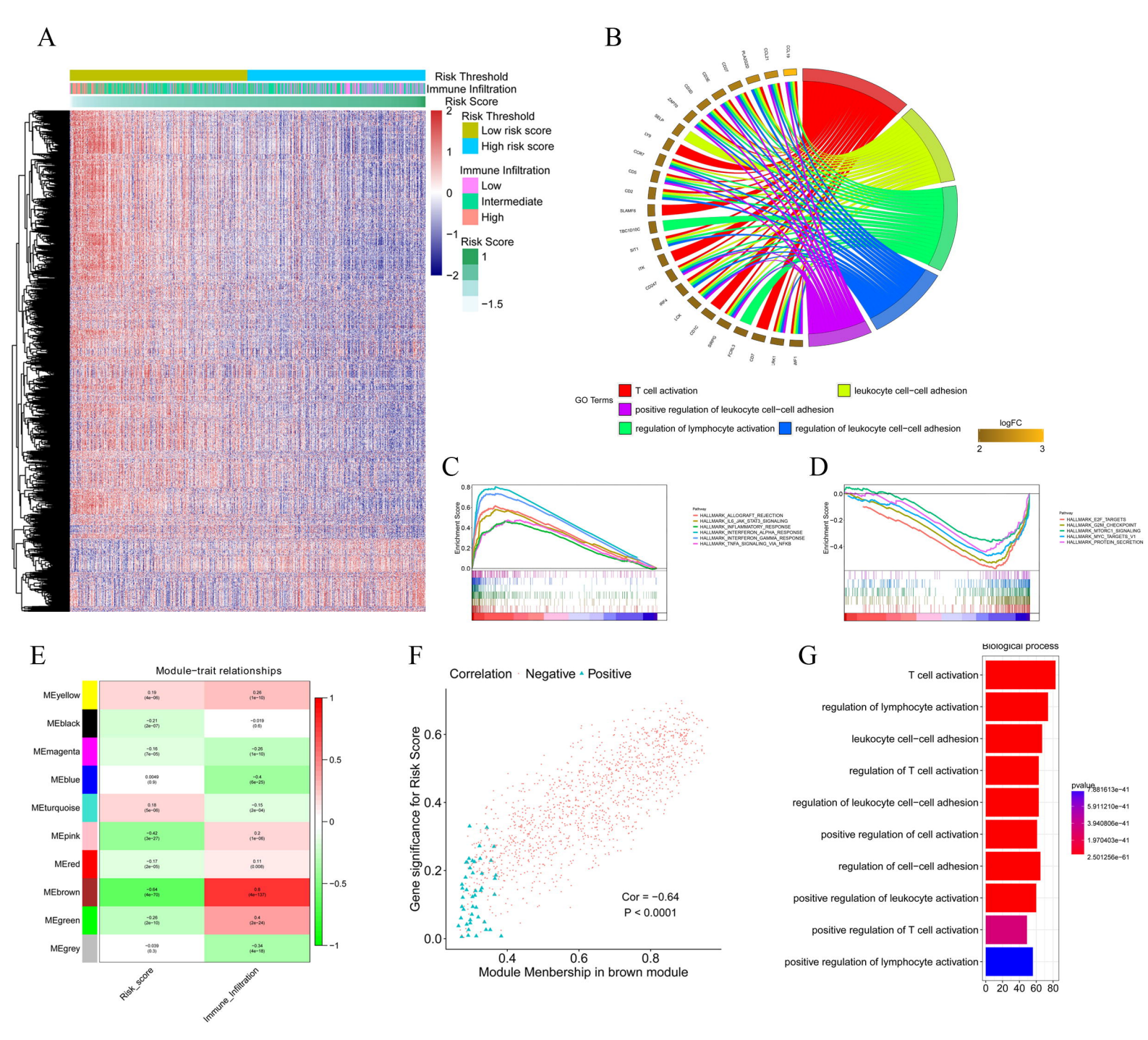
A
Risk Threshold
Immune Infiltration
Risk Score
Risk Threshold
Low risk score
High risk score
Immune Infiltration
Low
Intermediate
High
Risk Score
B
GO Terms
T cell activation
leukocyte cell−cell adhesion
positive regulation of leukocyte cell−cell adhesion
regulation of lymphocyte activation
regulation of leukocyte cell−cell adhesion
logFC
C
Enrichment Score
HALLMARK_ALLOGRAFT_REJECTION
HALLMARK_IL6_JAK_STAT3_SIGNALING
HALLMARK_INFLAMMATORY_RESPONSE
HALLMARK_INTERFERON_ALPHA_RESPONSE
HALLMARK_INTERFERON_GAMMA_RESPONSE
HALLMARK_TNFA_SIGNALING_VIA_NFKB
D
Enrichment Score
HALLMARK_E2F_TARGETS
HALLMARK_G2M_CHECKPOINT
HALLMARK_MTORC1_SIGNALING
HALLMARK_MYC_TARGETS_V1
HALLMARK_PROTEIN_SECRETION
E
Module−trait relationships
MEyellow
MEblack
MEmagenta
MEblue
MEturquoise
MEpink
MEred
MEbrown
MEgreen
MEgrey
Risk_score
Immune_Infiltration
F
Correlation · Negative ▲ Positive
Gene significance for Risk Score
Module Menbership in brown module
Cor = −0.64
P < 0.0001
G
Biological process
T cell activation
regulation of lymphocyte activation
leukocyte cell−cell adhesion
regulation of T cell activation
regulation of leukocyte cell−cell adhesion
positive regulation of cell activation
regulation of cell−cell adhesion
positive regulation of leukocyte activation
positive regulation of T cell activation
positive regulation of lymphocyte activation
pvalue

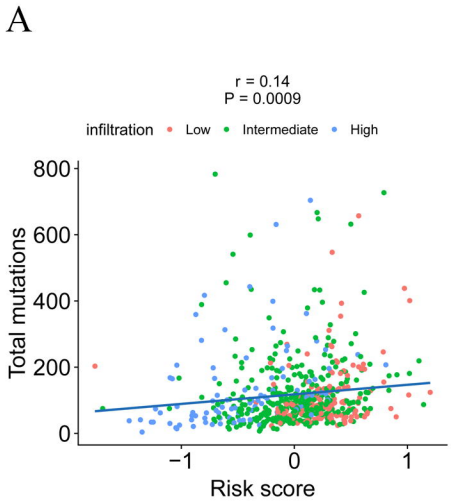
A
r = 0.14
P = 0.0009
infiltration Low Intermediate High
Total mutations
Risk score

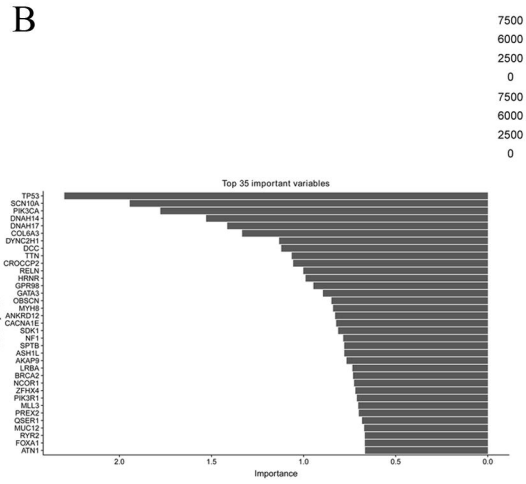
B
Top 35 important variables
Gene Symbol
Importance

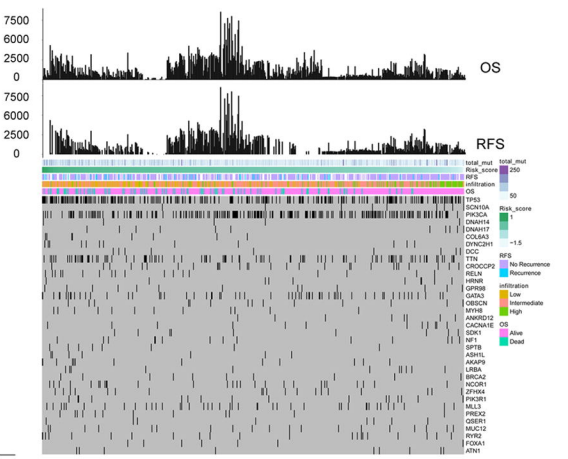
OS
RFS
total_mut
Risk_score
RFS
infiltration
OS
RFS
No Recurrence
Recurrence
infiltration
Low
Intermediate
High
OS
Alive
Dead

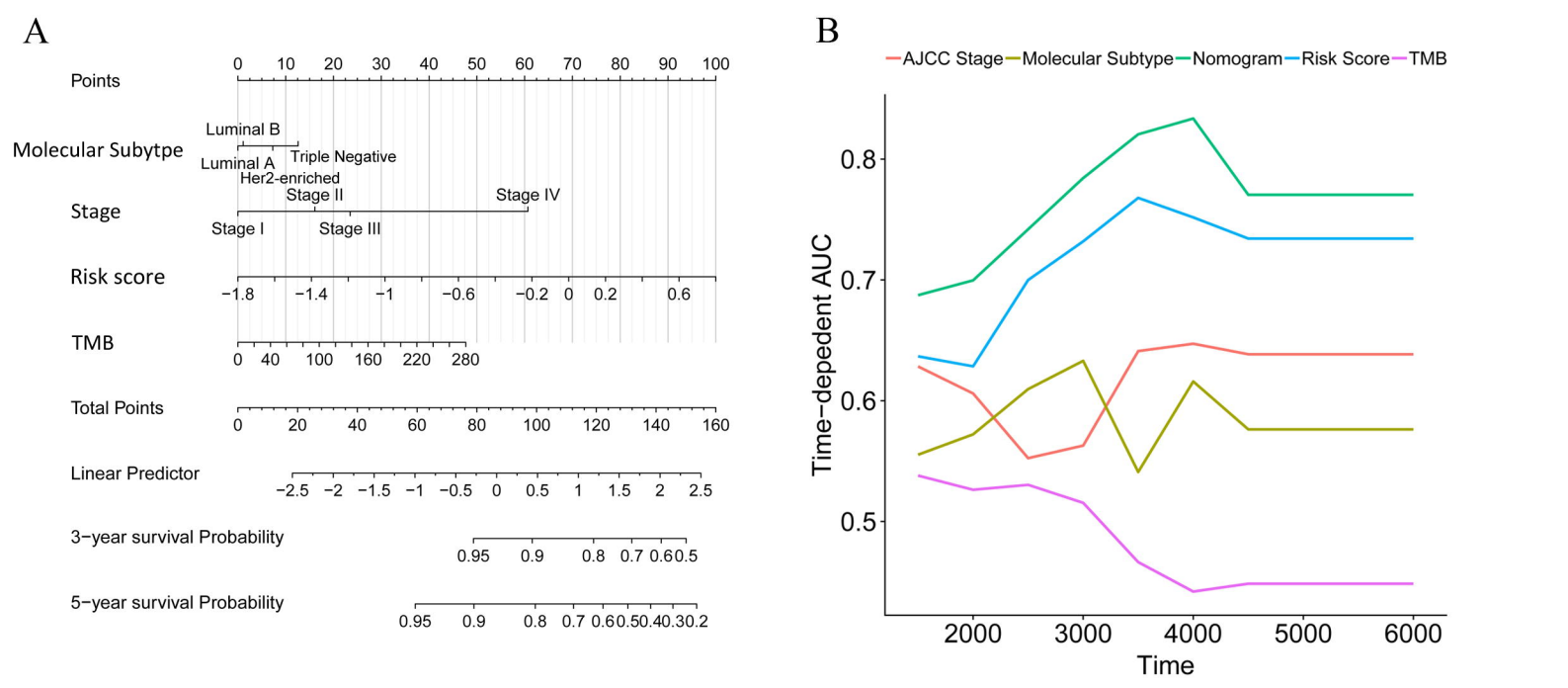
A
Points
0 10 20 30 40 50 60 70 80 90 100
Molecular Subytpe
Luminal B
Luminal A
Triple Negative
Her2-enriched
Stage
Stage II
Stage IV
Stage I
Stage III
Risk score
−1.8 −1.4 −1 −0.6 −0.2 0 0.2 0.6
TMB
0 40 100 160 220 280
Total Points
0 20 40 60 80 100 120 140 160
Linear Predictor
−2.5 −2 −1.5 −1 −0.5 0 0.5 1 1.5 2 2.5
3−year survival Probability
0.95 0.9 0.8 0.7 0.6 0.5
5−year survival Probability
0.95 0.9 0.8 0.7 0.6 0.5 0.4 0.3 0.2
B
AJCC Stage
Molecular Subtype
Nomogram
Risk Score
TMB
Time−depedent AUC
0.8
0.7
0.6
0.5
2000 3000 4000 5000 6000
Time

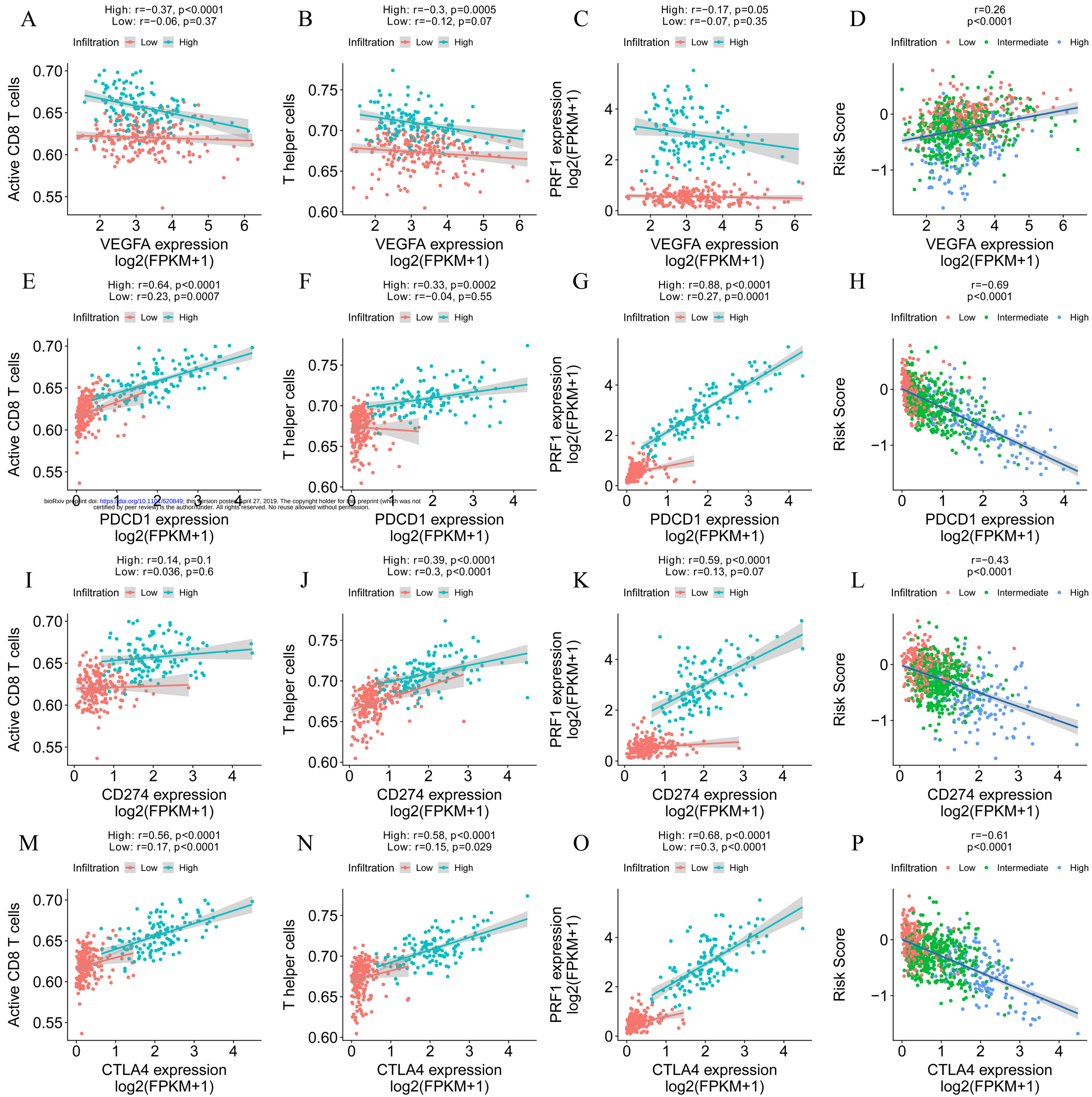

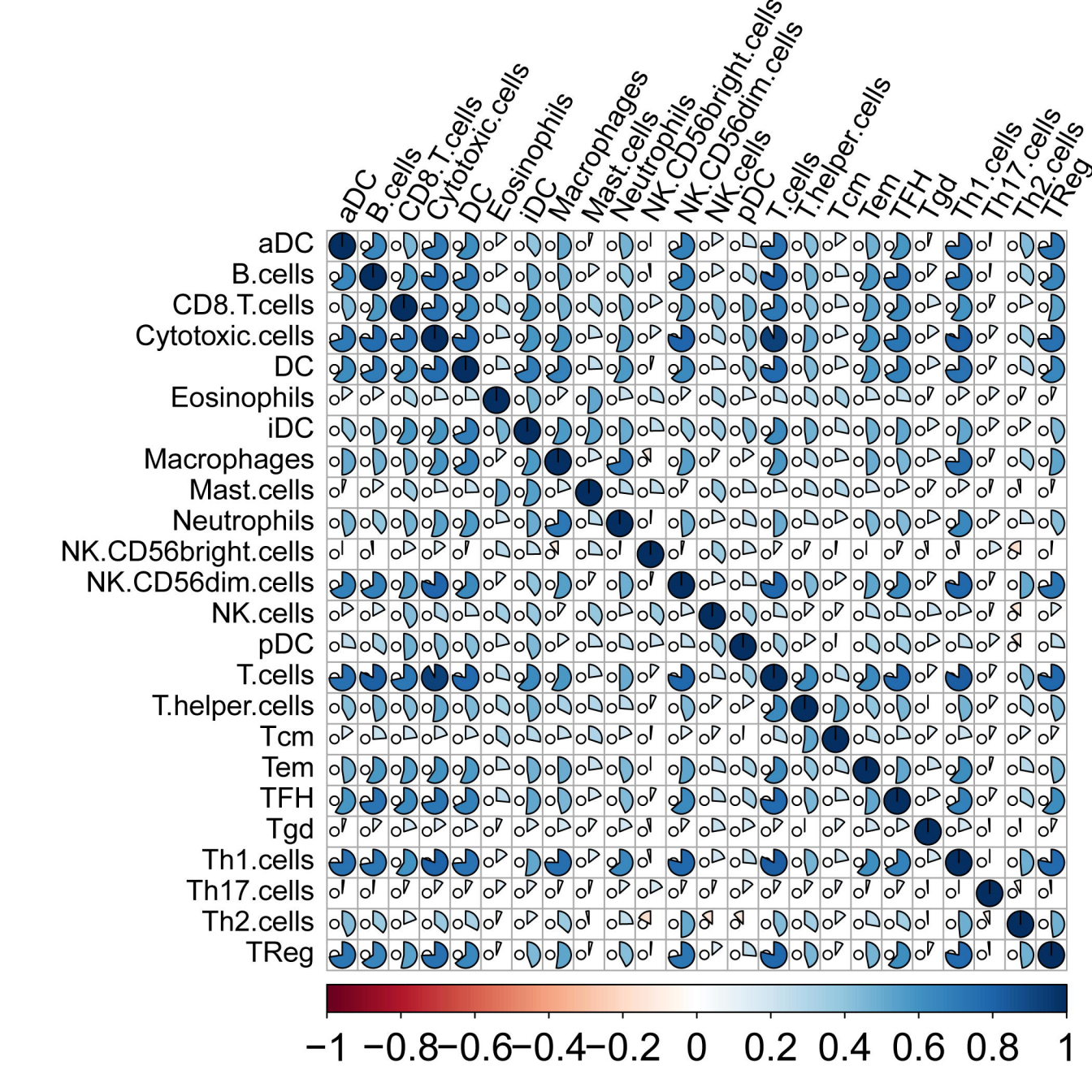
aDC
B.cells
CD8.T.cells
Cytotoxic.cells
DC
Eosinophils
iDC
Macrophages
Mast.cells
Neutrophils
NK.CD56bright.cells
NK.CD56dim.cells
NK.cells
pDC
T.cells
T.helper.cells
Tcm
Tem
TFH
Tgd
Th1.cells
Th17.cells
Th2.cells
TReg
−1
−0.8
−0.6
−0.4
−0.2
0
0.2
0.4
0.6
0.8
1

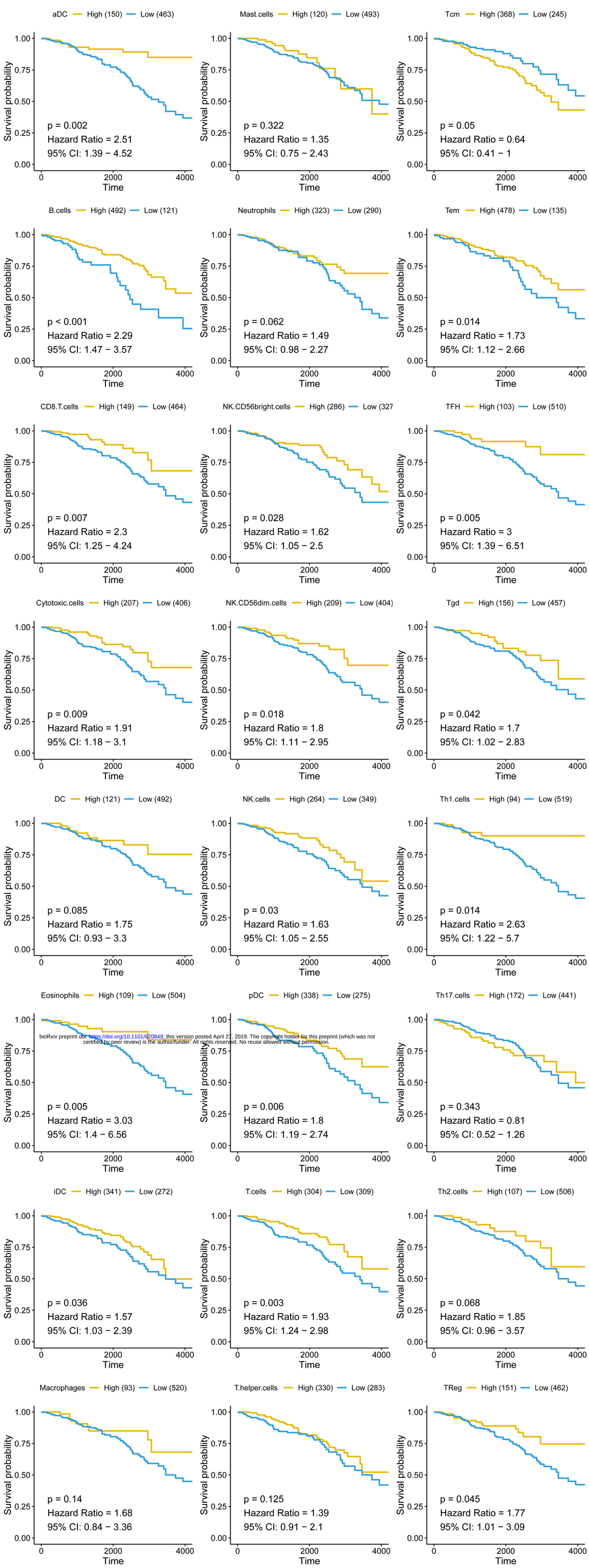

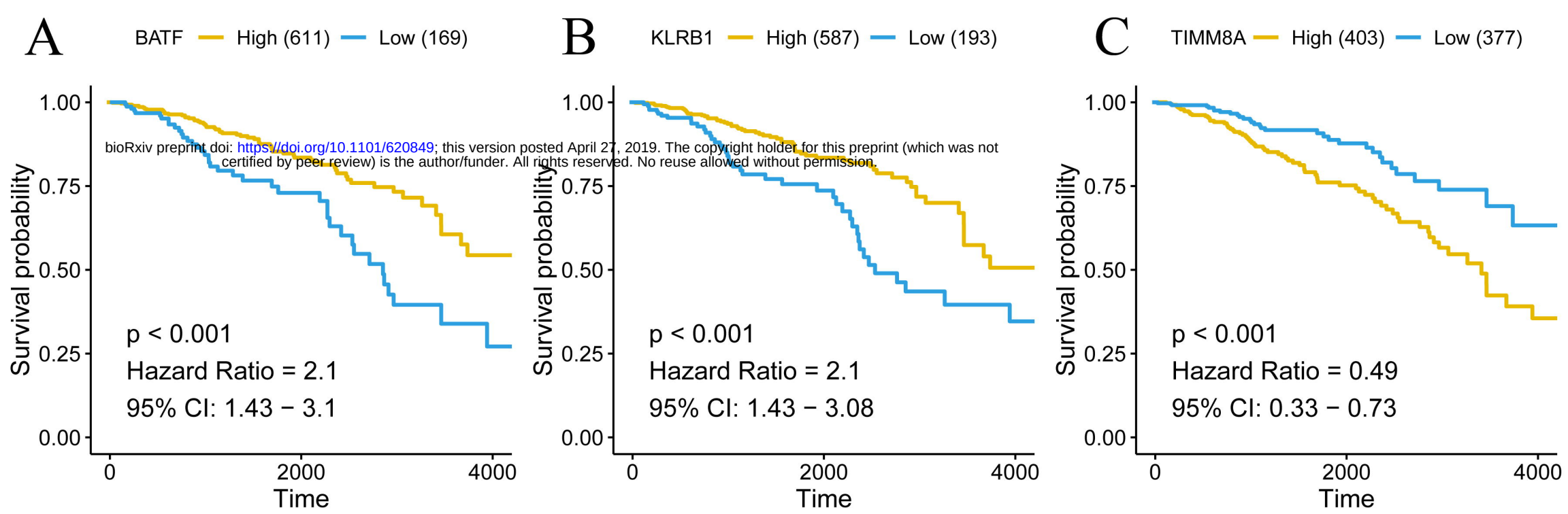

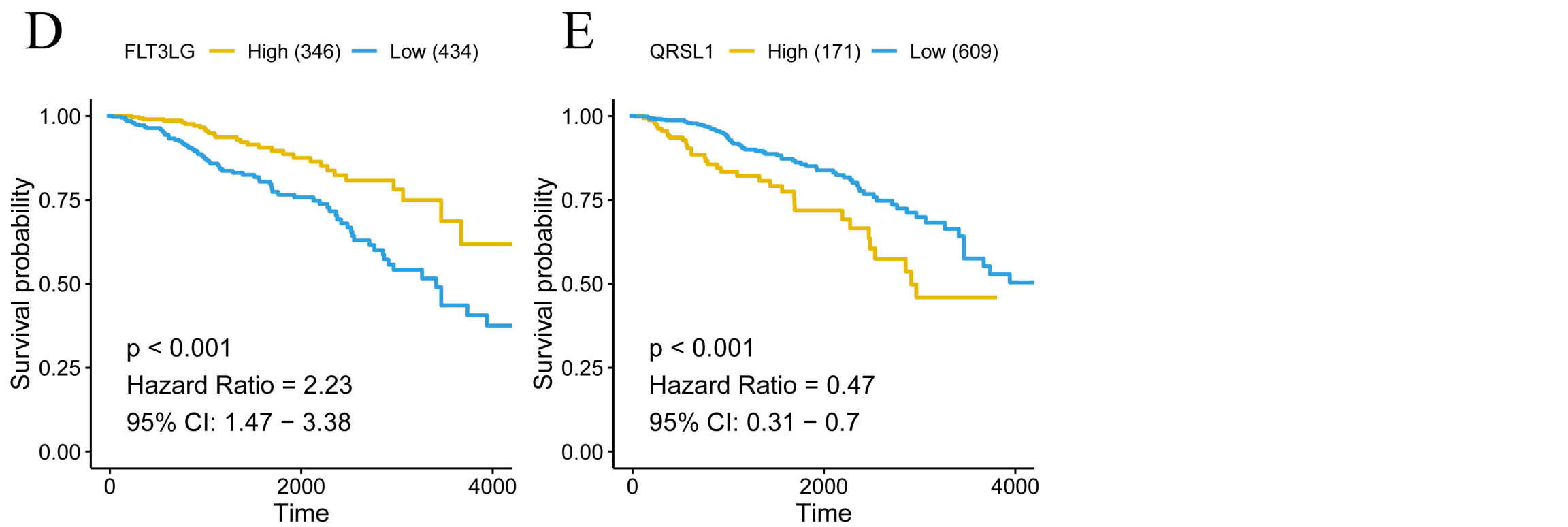

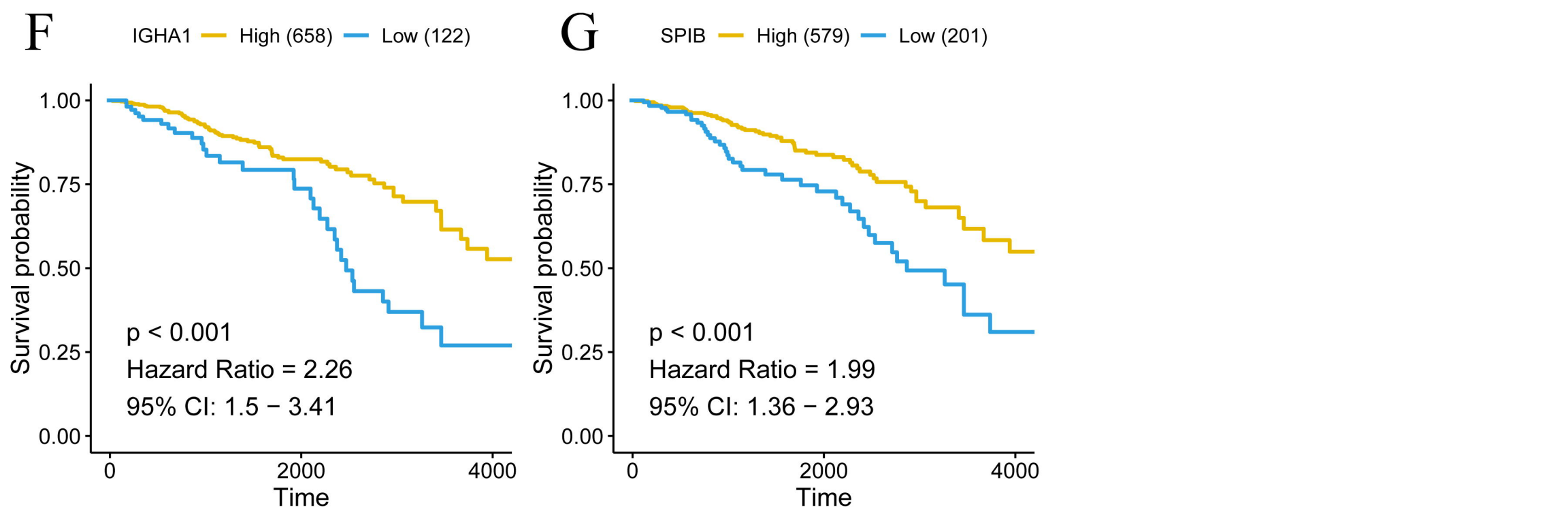

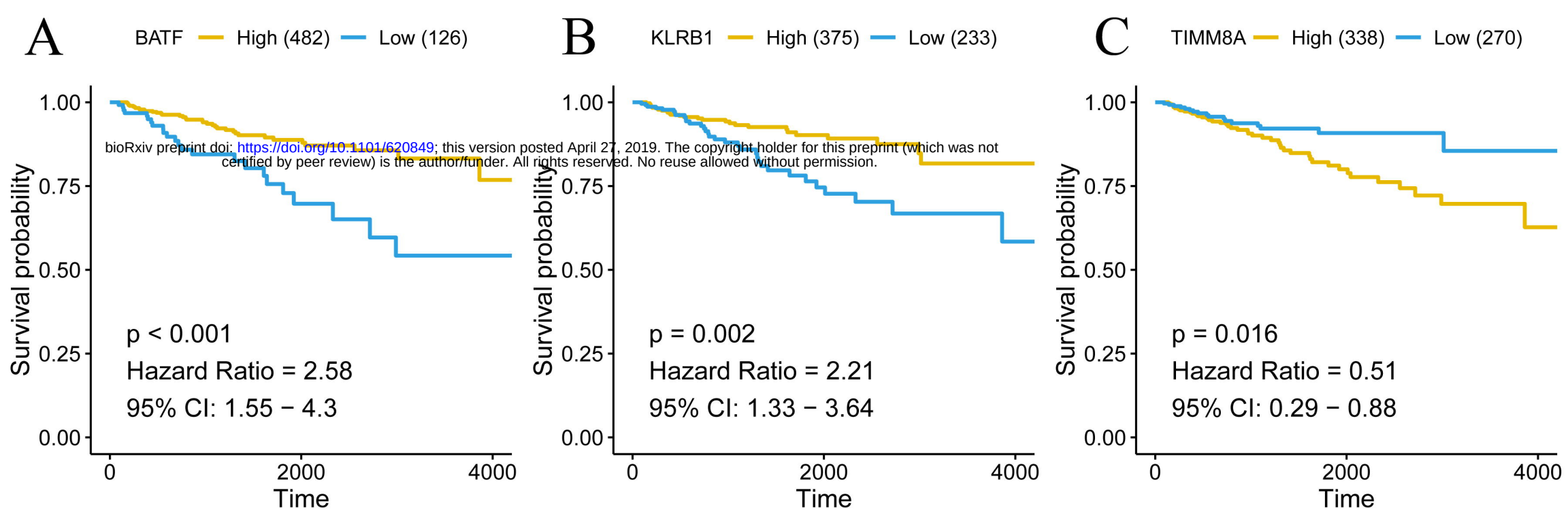

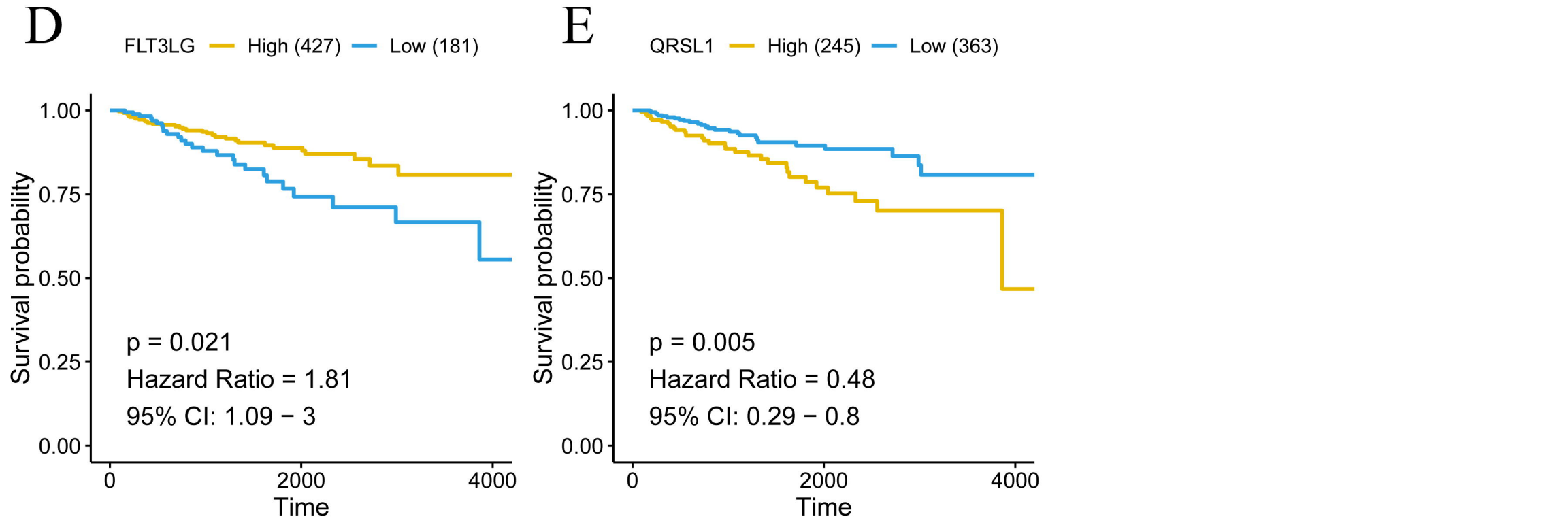

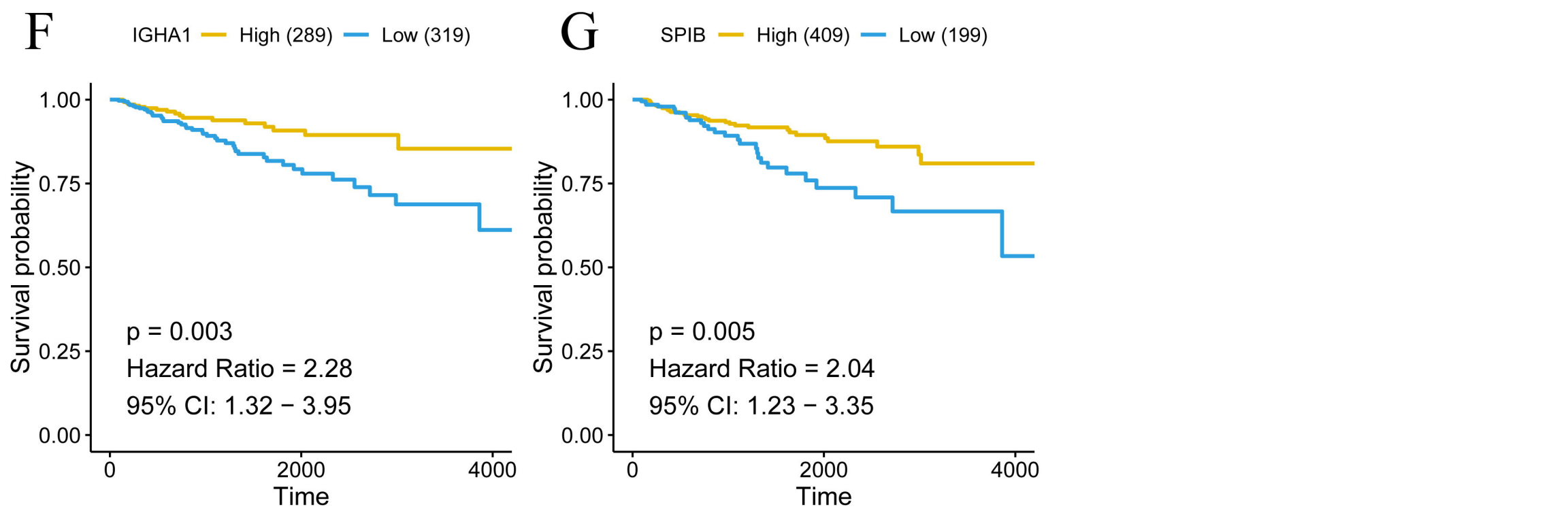

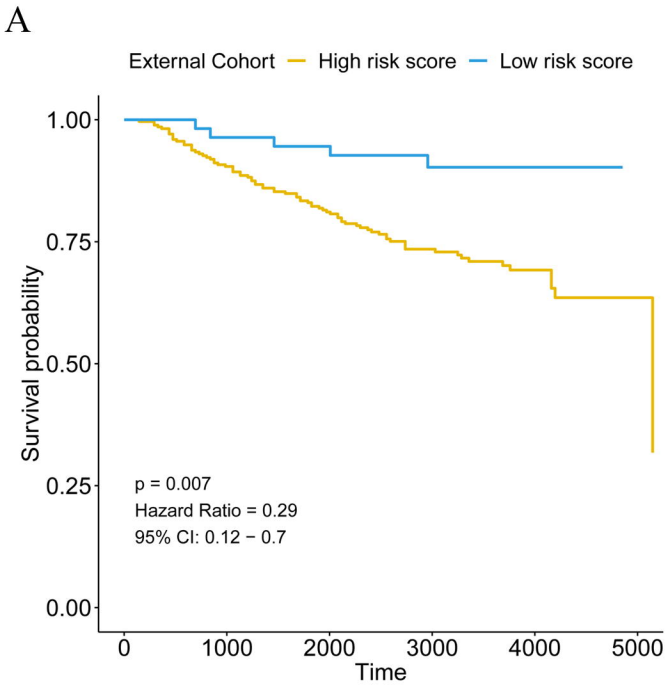
A
External Cohort
High risk score
Low risk score
1.00
0.75
0.50
0.25
0.00
Survival probability
p = 0.007
Hazard Ratio = 0.29
95% CI: 0.12 − 0.7
0
1000
2000
3000
4000
5000
Time

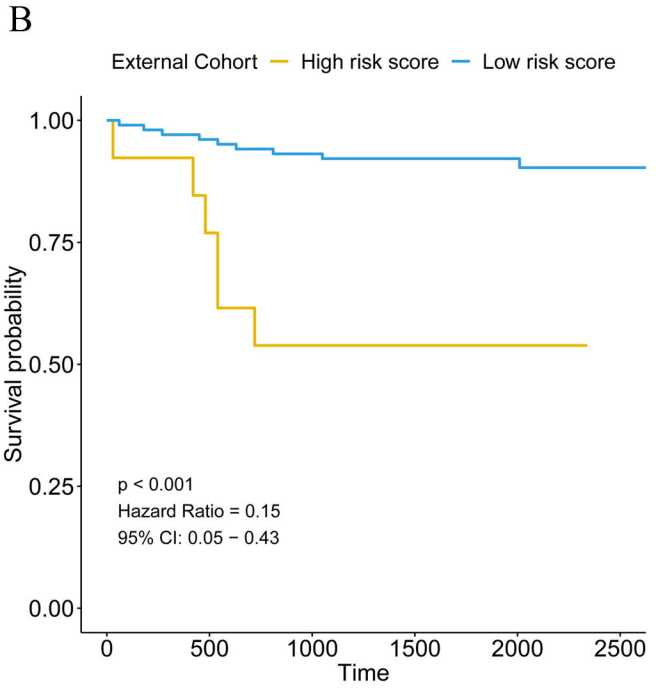
B
External Cohort
High risk score
Low risk score
1.00
0.75
0.50
0.25
0.00
Survival probability
p < 0.001
Hazard Ratio = 0.15
95% CI: 0.05 − 0.43
0
500
1000
1500
2000
2500
Time

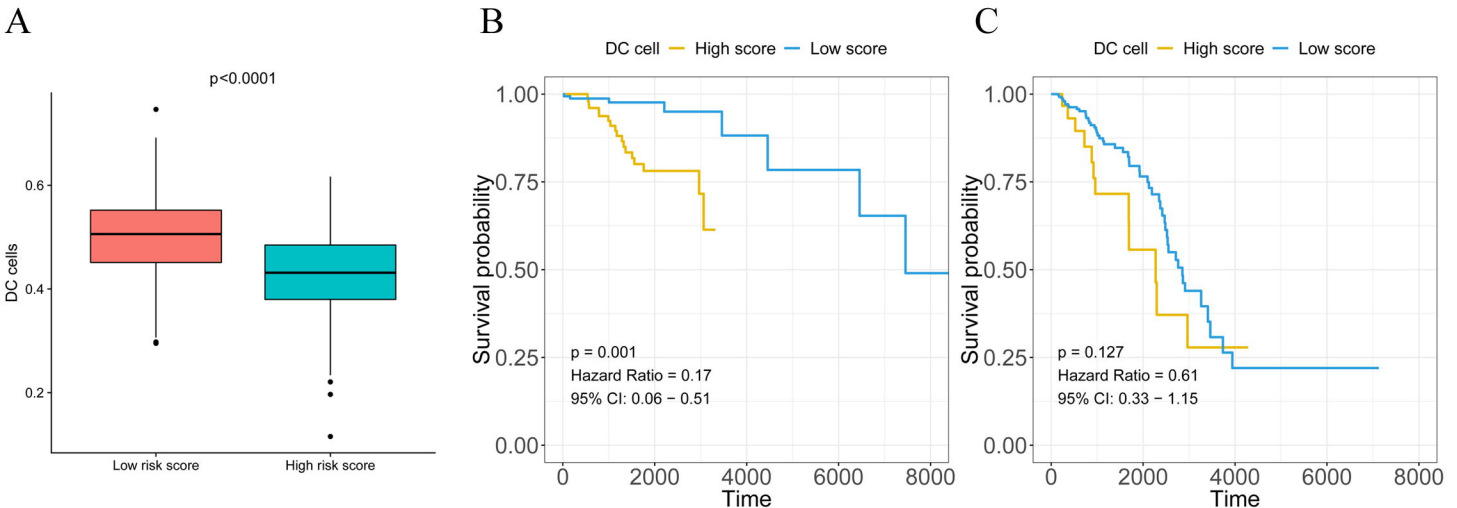
A
p<0.0001
DC cells
0.6
0.4
0.2
Low risk score
High risk score
B
DC cell
High score
Low score
Survival probability
1.00
0.75
0.50
0.25
0.00
p = 0.001
Hazard Ratio = 0.17
95% CI: 0.06 − 0.51
0
2000
4000
6000
8000
Time
C
DC cell
High score
Low score
Survival probability
1.00
0.75
0.50
0.25
0.00
p = 0.127
Hazard Ratio = 0.61
95% CI: 0.33 − 1.15
0
2000
4000
6000
8000
Time

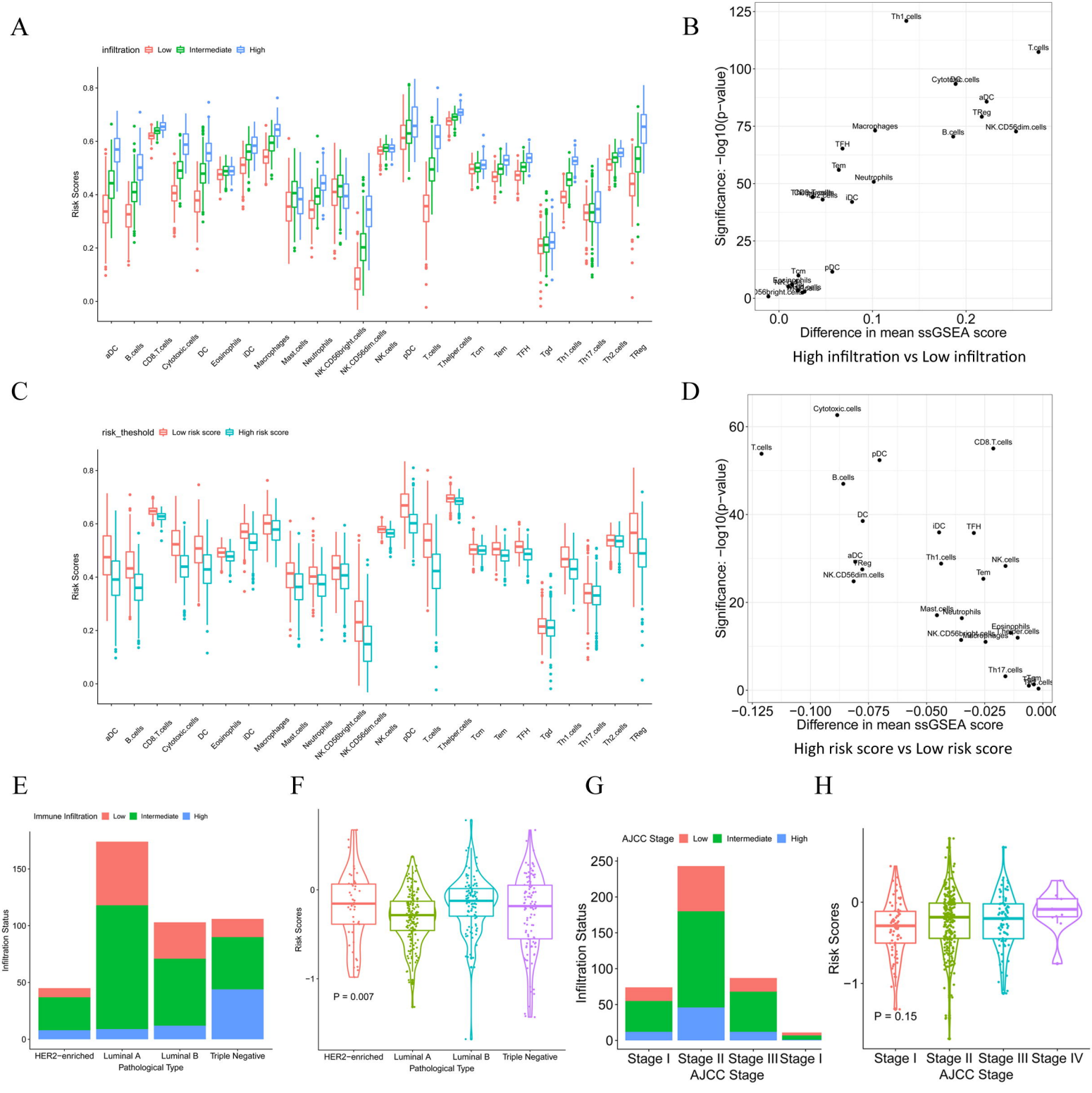
A
infiltration Low Intermediate High
Risk Scores
aDC B.cells CD8.T.cells Cytotoxic.cells DC Eosinophils iDC Macrophages Mast.cells Neutrophils NK.CD56bright.cells NK.CD56dim.cells NK.cells pDC T.cells T.helper.cells Tcm Tem TFH Tgd Th1.cells Th17.cells Th2.cells TReg
B
Significance: −log10(p−value)
Difference in mean ssGSEA score
High infiltration vs Low infiltration
C
risk_theshold Low risk score High risk score
Risk Scores
D
Significance: −log10(p−value)
Difference in mean ssGSEA score
High risk score vs Low risk score
E
Immune Infiltration Low Intermediate High
Infiltration Status
HER2−enriched Luminal A Luminal B Triple Negative
Pathological Type
F
Risk Scores
P = 0.007
HER2−enriched Luminal A Luminal B Triple Negative
Pathological Type
G
AJCC Stage Low Intermediate High
Infiltration Status
Stage I Stage II Stage III Stage I
AJCC Stage
H
Risk Scores
P = 0.15
Stage I Stage II Stage III Stage IV
AJCC Stage

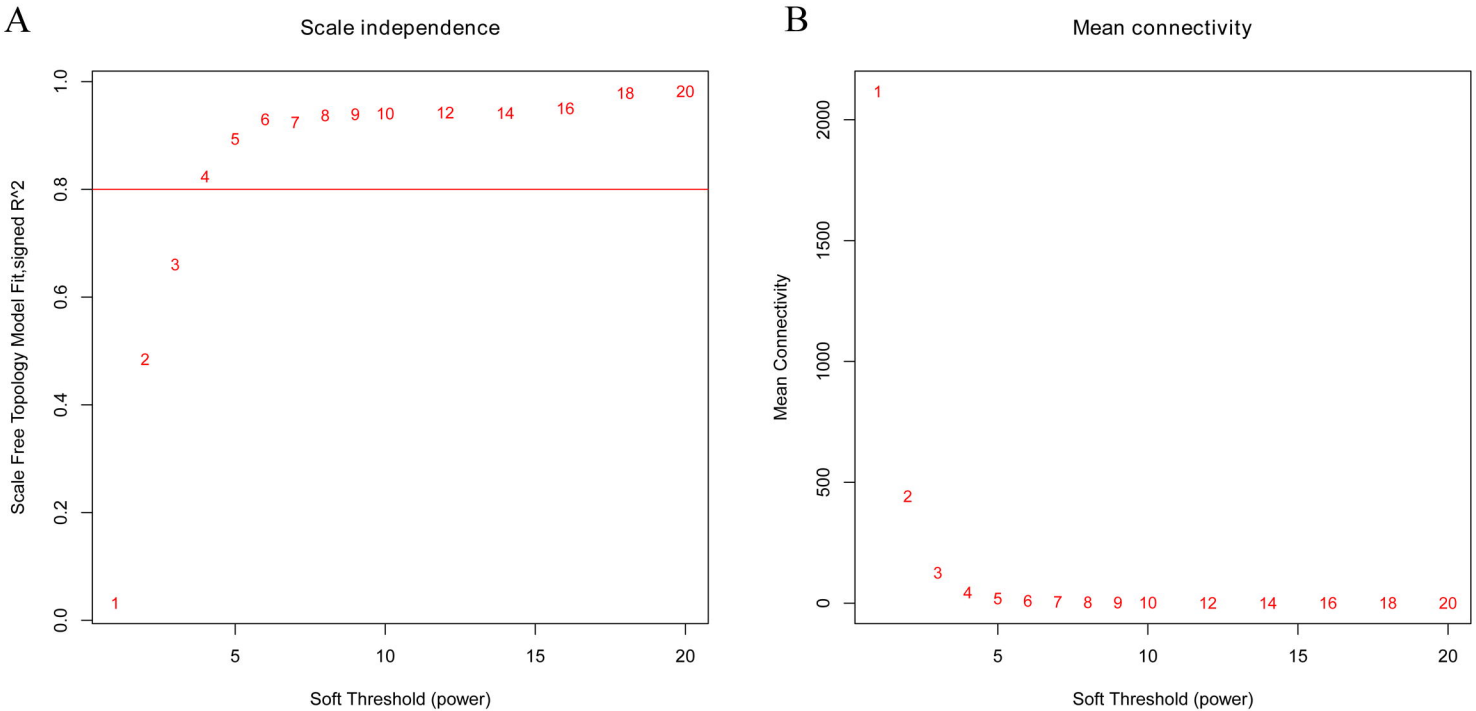
A
Scale independence
Scale Free Topology Model Fit,signed R^2
0.0
0.2
0.4
0.6
0.8
1.0
1
2
3
4
5
6
7
8
9
10
12
14
16
18
20
5
10
15
20
Soft Threshold (power)
B
Mean connectivity
Mean Connectivity
0
500
1000
1500
2000
1
2
3
4
5
6
7
8
9
10
12
14
16
18
20
5
10
15
20
Soft Threshold (power)

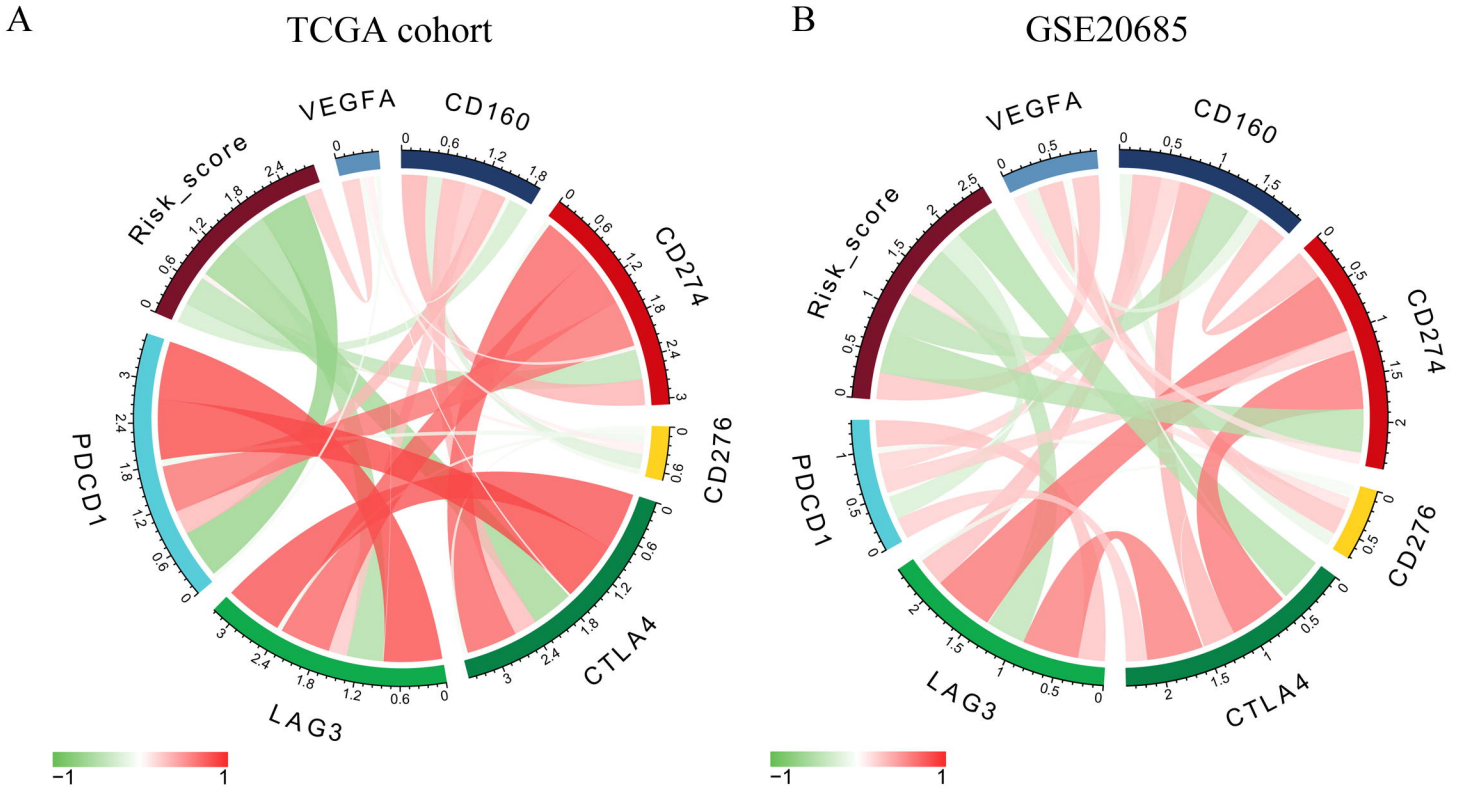
A
TCGA cohort
VEGFA
CD160
CD274
CD276
CTLA4
LAG3
PDCD1
Risk_score
−1
1
B
GSE20685
VEGFA
CD160
CD274
CD276
CTLA4
LAG3
PDCD1
Risk_score
−1
1